Calving front monitoring at sub-seasonal resolution: a deep learning application to Greenland glaciers

Erik Loebel[1], Mirko Scheinert[1], Martin Horwath[1], Angelika Humbert[2,3], Julia Sohn[2,4], Konrad Heidler[5], Charlotte Liebezeit[1], and Xiao Xiang Zhu[5]

[1]Technische Universität Dresden, Institut für Planetare Geodäsie, Dresden, Germany
[2]Alfred-Wegener-Institut Helmholtz Zentrum für Polar- und Meeresforschung, Sektion Glaziologie, Bremerhaven, Germany
[3]Universität Bremen, Fachbereich Geowissenschaften, Bremen, Germany
[4]IU Internationale Hochschule, Erfurt, Germany
[5]Technische Universität München, Chair for Data Science in Earth Obervation, München, Germany

Correspondence: Erik Loebel (erik.loebel@tu-dresden.de)

Abstract. The mass balance of the Greenland ice sheet is strongly influenced by the dynamics of its outlet glaciers. Therefore, it is of paramount importance to accurately and continuously monitor these glaciers, especially the variation of their frontal positions. A temporally comprehensive parameterization of glacier calving is essential to understand dynamic changes and to constrain ice sheet modelling. However, current calving front records are often limited in temporal resolution as they rely on manual delineation, which is laborious and not feasible with the increasing amount of satellite imagery available. In this contribution, we address this problem by applying an automated method to extract calving fronts from optical satellite imagery. The core of this workflow builds on recent advances in the field of deep learning while taking full advantage of multispectral input information. The performance of the method is evaluated using three independent ~~validation datasets.~~ test datasets. We calculate a mean delineation error of $61.2\,\mathrm{m}$, $73.7\,\mathrm{m}$, and $73.5\,\mathrm{m}$, respectively. Eventually, we apply the technique to Landsat-8 imagery. We generate 9243 calving front positions across 23 Greenland outlet glaciers from 2013 to 2021. Resulting time series resolve not only long-term and seasonal signals but also sub-seasonal patterns. We discuss the implications for glaciological studies and present a first application ~~analysing the interaction between calving front variation and bedrock topography~~ to the analysis of the effect of bedrock topography on calving front variations. Our method and derived results represent an important step towards the development of intelligent processing strategies for glacier monitoring, opening up new possibilities for studying and modelling the dynamics of Greenland outlet glaciers. ~~Thus, these also contribute to advance the construction of a digital twin of the Greenland ice sheet, which will improve our understanding of its evolution and role within the Earth's climate system.~~

1 Introduction

Over the past two decades, the Greenland Ice Sheet has been a major contributor to sea level rise (Horwath et al., 2022). Models suggest, that this imbalance will continue with a warming climate (Goelzer et al., 2020; Edwards et al., 2021; Rückamp et al., 2020). About half of the ice mass loss is due to increased meltwater runoff, while the other half is caused by dynam-

ical imbalance ~~(The IMBIE Team, 2020)~~(Otosaka et al., 2023). While changes in the surface mass balance are forced by the atmosphere, the dynamic imbalance is driven by changes at the ice-ocean boundary formed by the outlet glaciers that drain the Greenland Ice Sheet. Here, several mechanisms act as controls and indicators for dynamic glacier changes. In particular, calving and calving front variations have been identified as crucial parameters for investigating the physical mechanisms of Greenland outlet glaciers (Joughin et al., 2008a; Moon and Joughin, 2008; Benn et al., 2017; Trevers et al., 2019; Cook et al., 2021; Melton et al., 2022). In addition, recent studies have shown that calving front retreat is associated with increased ice discharge (King et al., 2018; Mouginot et al., 2019; King et al., 2020). An accurate representation of calving front behaviour is therefore an important requirement for constraining ice sheet modelling and improving simulations of future mass loss and sea level contribution (Vieli and Nick, 2011; Bondizo et al., 2017; Morlighem et al., 2017, 2019). Overall, temporally and spatially comprehensive data products of calving front variation are essential for a better understanding and modelling of marine terminating glaciers.

The steady increase in quality and availability of satellite imagery provides new opportunities for a continuous and accurate monitoring of glacier calving front positions. Nevertheless, current data records mostly rely on manual delineation (Schild and Hamilton, 2013; Joughin et al., 2015; ENVEO, 2017; Andersen et al., 2019; King et al., 2020; Goliber et al., 2022; Black and Joughin, 2023). This is a laborious, time-consuming and therefore ineffective process, given the ever-increasing volume of data. Thus, such calving front products often lack temporal resolution, making seasonal analysis and associated modelling efforts difficult. In response to the need for scalable processing strategies, several empirical feature extraction algorithms have been introduced over the last decades, all aiming to provide robust automated calving front extraction (Sohn and Jezek, 1999; Liu and Jezek, 2004; Seale et al., 2011; Rosenau, 2014; Krieger and Floricioiu, 2017; Liu et al., 2021). Yet, most of these methods are either not tested for spatial transferability and large-scale application, or require case-specific modifications.

With the advent of deep learning and big data methods in remote sensing, new opportunities have emerged to solve complex image processing tasks (Zhu et al., 2017). In recent years, a number of case studies have used deep Artificial Neural Networks (ANN) to extract calving front positions. Both optical (Mohajerani et al., 2019) and synthetic aperture radar (SAR) (Zhang et al., 2019; Baumhoer et al., 2019) sensors have been used. Based on ~~this~~these case studies, numerous studies have advanced the ANN architecture ~~(Heidler et al., 2021; Marochov et al., 2021; Periyasamy et al., 2022; Davari et al., 2022b,a; Heidler et al., 2022)~~ ,(Heidler et al., 2021; Marochov et al., 2021; Periyasamy et al., 2022; Davari et al., 2022b,a; Heidler et al., 2023; Herrmann et al., 2023; V , have assessed potential input information (Loebel et al., 2022) and have pursued the multi-sensor capability (Zhang et al., 2021). In addition, dedicated data products have been developed for training and validation (Goliber et al., 2022) as well as benchmarking (Gourmelon et al., 2022) of ANN applications. ~~Cheng et al. (2021) published the first and only~~ The results from Cheng et al. (2021) and Zhang et al. (2023), namely the CALFIN and AutoTerm repositories, are currently the only two automatically generated data ~~product~~ sets of calving front locations with a ~~Greenlandic~~ Greenland-wide scope.

Building on these achievements, this paper discusses the application and extensive validation of a specially tailored deep learning method for automated calving front extraction using Landsat-8 optical imagery. In doing so, we provide a data product for 23 Greenland outlet glaciers from 2013 to 2021. We compare this data product to CALFIN and AutoTerm repositories. By exploiting the full multispectral sensor information, ~~we achieve a more accurate and robust calving front extraction compared~~

to using only single band inputs. This significantly increases the temporal resolution of the final product. Thus, the time series of many of the glaciers processed are of unprecedented temporal resolution, resolving their sub-seasonal calving front variability for the first timeour method is able to extract a significant amount of calving fronts that could not be extracted by the other automation methods. By achieving this robust and comprehensive parameterization of glacier calving in Greenland, we meet the glaciology community requirement and make an important first step important steps towards establishing intelligent processing strategies for glacier monitoring tasks. Overall, we provide the wider cryosphere community with a methodology, a data product and implementation, a comparison to existing products, as well as a discussion of glaciological implicationsthat open up new possibilities for studying and modelling Greenland glacier dynamics.

Section 2 introduces the data and the applied deep learning method for automated calving front extractionand . Section 3 gives an assessment of its accuracy the accuracy of our method and its spatial transferability. In Section 4 we present our data productand , the derived time series and a comparison to existing data repositories. As part of the discussion in Section 5, we provide a first an application of our results to analyse the interaction between calving front change and bedrock topography. Finally, in Section 6 we draw conclusions and provide an outlook.

2 Delineating calving fronts by deep learningData and Methods

2.1 Neural network processing

For automated calving front extraction, we apply a modified version of the approach published by Loebel et al. (2022). In doing so, we process multispectral The presented processing system extracts glacier calving front shapefiles from multispectral Landsat-8 imagery. In this process, we use satellite imagery as reference data and apply a specialized ANN. This involves a series of processing steps and configurations which are explored in the following section.

2.1 Data source

Our processing system is based on optical Landsat-8 imagery(Appendix ??) using a specialized ANN (Appendix ??). In particular, we use a convolutional neural network of the U-Net architecture (Ronneberger et al., 2015) to semantically segment multispectral imagery into a glacier/land and water class. The glacier calving front, which is described by the boundary between these two classes, is then extracted by vectorizing and masking the model prediction. Figure 1 gives a broad overview of the processing workflow. Larger glaciers, exceeding the fixed window size, are processed by separating the region of interest into multiple independent predictions which are then averaged in the overlapping area prior to vectorization (Baumhoer et al., 2019) . The associated reference data (Appendix ??), which is instrumental both in training and validating machine learning applications, is build from . We use the orthorectified and radiometrically calibrated level 1 data products as provided by the United States Geological Survey (U.S. Geological Survey, 2023). Carrying two scientific instruments, the Operational Land Imager (OLI) and the Thermal Infrared Sensor (TIRS), Landsat-8 provides a particularly wide multispectral coverage. The eleven spectral bands comprise data from visible, near-infrared, short-wave infrared and thermal infrared wavelengths, from $0,435\,\mu m$ to

Figure 1. Overview map of the 23 Greenland glaciers used in the TUD reference dataset. Glaciers marked by a red dot are used for training and testing. White dots indicate glaciers only used for model testing. Not on this map: Boydell Glacier (Antarctica), Drygalski Glacier (Antarctica), Storbreen Glacier (Svalbard) and Upsala Glacier (Patagonia) which are only applied for model testing. The basemap is taken from the QGreenland package (Moon et al., 2022).

$1,384\,\mu m$. With exception to the panchromatic band and the two thermal bands, which have a spatial resolution of $15\,m$ and $100\,m$ respectively, all other bands have a resolution of $30\,m$. Apart from band 9, which is outside an atmospheric window and, therefore, intended for atmospheric observations, all available bands are used as input for our ANN. The integration of these multispectral bands leads to generally more accurate predictions than using conventional single-band inputs only, which has already been shown by Loebel et al. (2022). This is especially true for difficult illumination and ice-melange conditions.

2.2 Reference dataset

We use manually delineated calving front ~~positions. To train the ANN model~~ locations as reference data. For model training, we use 698 calving front ~~locations from~~ positions across 19 Greenland glaciers between 2013 and 2019. Glaciers are selected for their broad spatial distribution and diverse morphology as well as for different calving and ocean conditions. A spatial overview

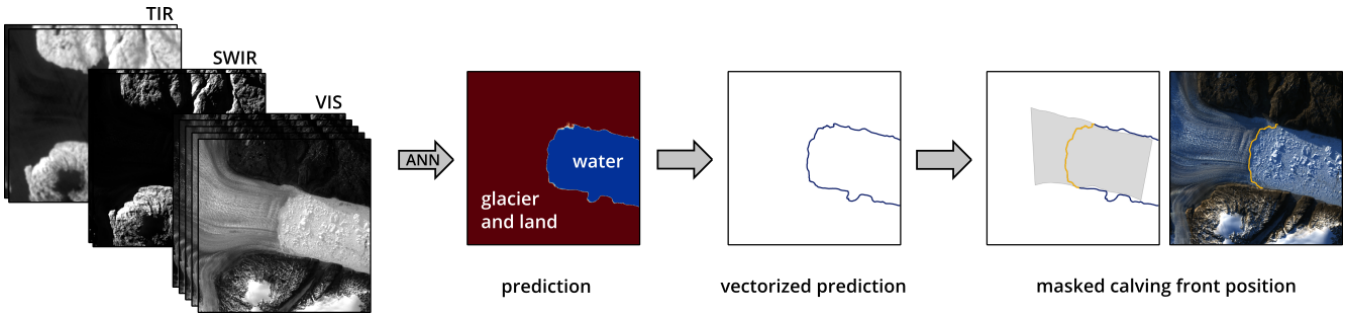

Figure 2. High-level overview of the applied workflow for automated calving front extraction. Based on multispectral satellite imagery in visible (VIS), short-wave infrared (SWIR) and thermal infrared (TIR) wavelengths, the ANN performs a pixel-wise semantic image segmentation. The final calving front position is obtained after vectorizing and masking the ANN prediction. Landsat-8 image courtesy of the U.S. Geological Survey.

of all Greenland glaciers applied in this study is given in Figure 1. As the performance of ANN methods highly depends on training data we pay special attention to cover a diversity of morphological features, terminus with heavy crevassing, different calving and ice mélange conditions as well as varying illumination and cloud situations. To test the model we apply three different testing sets. The TUD testing dataset includes four additional Greenland glaciers, Boydell and Drygalski Glacier at the Antarctic Peninsula, Storbreen Glacier in Svalbard as well as Upsala Glacier in Patagonia. In total, the TUD testing set contains 200 calving front positions across 27 glaciers from 2020 and 2021. In addition to our own testing data set we use manually delineated calving fronts from the ESA-CCI (ENVEO, 2017) and the CALFIN (Cheng et al., 2021) product. Here, we use all available calving front positions for our selected Greenland glaciers for which we find a corresponding Landsat-8 scene with less than 24 hours time difference. This results in additional 100 manually delineated calving front positions for the ESA-CCI and 110 for the CALFIN testing datasets.

2.3 Delineating calving fronts by deep learning

For automated calving front extraction, we apply a modified version of the approach published by Loebel et al. (2022). The main difference is, that we only use the multi-spectral information and no textural and topographic features. This reduces the input from 17 to nine layers. Additionally, we have expanded the reference data set by 170 entries. These new calving front traces focus specifically on cloudy, low illumination and scene border conditions, thereby enhancing the method in this regard. Figure 2 gives a broad overview of the processing workflow.

2.4 ~~Validation~~

~~Our~~

2.3.1 Pre-Processing

To use the satellite data as input for the ANN requires pre-processing. In particular, we create stacked raster subsets from the multispectral satellite bands and the manually delineated calving front locations. These subsets have dimensions of 512 px × 512 px with a unified 30 m ground sampling distance and are centered on the calving front of the respective glacier. For each multispectral band we apply an image enhancement in form of a cumulative count cut, clipping the data between the 0.1 and 98 percentile, counteracting overexposure in our satellite imagery. Additionally, all satellite bands are then normalized to the range between 0 and 1 using an 8-bit quantization. Corresponding manually delineated calving front positions, given either as a line string or polygon shape-file, are processed into binary raster masks segmenting land and glacier from ocean. Altogether, one stacked raster subset includes nine satellite bands and a matching ground truth mask.

2.3.2 Semantic image segmentation

To extract the calving front location from the input images we apply a convolutional neural network that performs a pixel-wise semantic image segmentation, separating a glacier-land class from a water class. In particular, we use a U-Net type architecture introduced by Ronneberger et al. (2015). This architecture consists of a contracting path, resembling a typical convolutional network where spatial resolution is reduced while feature information is increased, followed by an expanding path where feature and spatial information are combined. The receptive field of a U-Net is defined by the number of contracting and expanding blocks. As calving front extraction needs adequate spatial context (Heidler et al., 2021) in this study we enhance the U-Net by two additional resolution levels, i.e. from four to six.

Our model is fitted using the pre-processed training data. Before initializing the model training we select every fifth image of the training dataset for internal validation. The remaining training data is augmented eightfold by rotating and flipping. Finally, the resulting 6208 raster subsets are used for fitting the model. For this, we use randomized batches of size eight and apply the Adam optimization algorithm (Kingma and Ba, 2014) on a binary cross-entropy loss function for a total of 200 epochs. Final model weights are selected based on the classification accuracy of the internal validation dataset.

The ANN processing is implemented using the TensorFlow 2.4 library (Abadi et al., 2015). Model training is carried out on an IBM Power 9 node and an NVIDIA V100 GPU with 32 GB high bandwidth memory. The training of one model requires about twelve hours with a main memory utilization of 80 GB and an average GPU power consumption of 265 W.

2.3.3 Post-Processing

As output of the ANN output we derive a floating point number probability mask where each image pixel is assigned a probability between 0 (water) and 1 (glacier and land). During post-processing, we vectorize this probability mask using the Geospatial Data Abstraction Library (GDAL) contour algorithm (GDAL/OGR contributors, 2020) with a threshold of 0.5 and separate the longest feature. Eventually, we extract the glacier's calving front by intersecting the vectorized coastline trajectory with a static mask. This mask is created manually for each glacier and specifies a corridor of possible calving front locations. Calving fronts exceeding the 512 px × 512 px window are split into multiple independent predictions which are then averaged in the overlapping area before vectorization. Applying this strategy, which is motivated by Baumhoer et al. (2019), Zachariae

Isstrøm, Nioghalvfjerdsbrae and Humboldt Glacier are split into two, three and seven separate overlapping predictions, respectively.

3 Accuracy assessment

Our own TU Dresden (TUD) testing set contains 200 labeled images from the years 2020 and 2021. We emphasize that they are temporally separated from the years of the training datasets. To ensure spatial transferability of our method this ~~validation~~ test data set includes imagery for additional four Greenland glaciers, two glaciers at the Antarctic Peninsula, one glacier in Svalbard and one glacier in Patagonia. In addition to our own testing dataset we apply another 100 manually picked calving fronts provided by the ESA Greenland Ice Sheet CCI project (ENVEO, 2017) and 110 provided by the CALFIN product (Cheng et al., 2021). ~~Figure 2 gives a spatial overview of the Greenland glaciers used within this study. Overview map of the 23 Greenland glaciers used in the TUD reference dataset. Glaciers marked by a red dot are used for training and testing. White dots indicate glaciers only used for model testing. Not on this map: Boydell Glacier, Drygalski Glacier, Storbreen Glacier and Upsala Glacier which are only applied for model testing. The basemap is taken from the QGreenland package (Moon et al., 2022).~~

3.1 Error Estimation

~~Accuracy assessment for the three independent test datasets. Every horizontal line inside the 'violin graphs' represents one trained model applied to the test dataset. The vertical extent of each graph is defined by the corresponding minimum and maximum values.~~ The distance between the predicted and the manually delineated calving front is taken as the main error ~~metric in the validation. This is implemented~~ measure in the model testing. We calculate the average minimal distance error by averaging the minimal distances between the predicted front trajectory and the manual delineation calculated every 30 m. Our definition of the average minimal distance error is comparable to the estimates used by Cheng et al. (2021) and Zhang et al. (2023). Figure 3 illustrates some ~~validation~~ test results for diverse testing images from the three ~~validation~~ test sets. Along with the manually picked calving front (dashed black) and the ANN delineated calving front (orange) the ~~mean~~ average distance between them is indicated. The ANN model reliably delineates calving front locations under a wide range of ocean, sea ice and ice mélange situations. Furthermore, the model is also able to handle images affected by challenging cloud (Fig. 3d, j) and illumination (Fig. 3c) conditions, as well as calving fronts near the edge of a satellite scene (Fig. 3e). ~~Validation~~ Test images showing large errors are associated to delineation subjectivity (Fig. 3f,h,i) or even human error (Fig. 3k).

Since the ANN training is stochastic every fitted model performs slightly different on our testing data. To ensure statistical stability for a broader numerical assessment we train and ~~validate~~ test 50 models using the same reference data and model parameters. In order to assess the distance error, we report both the mean and median over the scenes in the test data set. The ~~validation~~ test results for these 50 models are shown in Figure 4. Whereas the mean distance error is sensitive towards outliers the median distance error informs about systematic model overfitting and general scene-by-scene performance. Since each of the three testing data sets originated from its own, hence independent, imagery, resulting error estimates are not directly

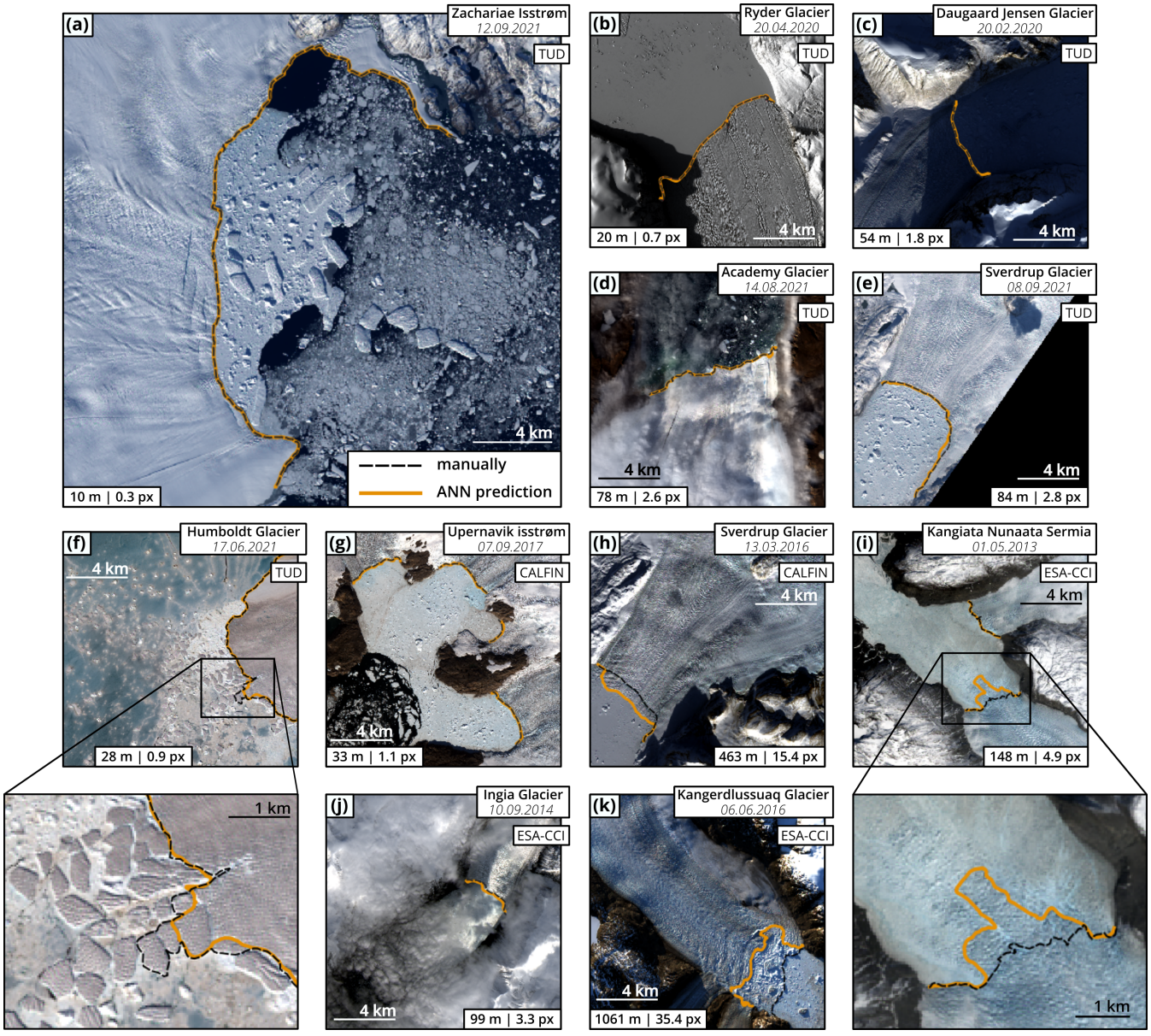

Figure 3. ~~Validation~~ Test results for example scenes from the (a-f) TUD, (g,h) CALFIN and (i-k) ESA-CCI testing set. Manually delineated calving fronts are depicted as dashed black lines. The ANN prediction is shown in orange. The mean average minimal distance error for the respective scene is given both in meters and in pixels. All depicted results derive from the same fitted ANN model. Landsat-8 imagery courtesy of the U.S. Geological Survey.

180 comparable. Nevertheless, we suspect that the lower distance error yielded for the TUD testing set is due to the fact that it was generated by the same people who inferred the training data for these models. ~~For all three testing sets the ANN mean distance~~

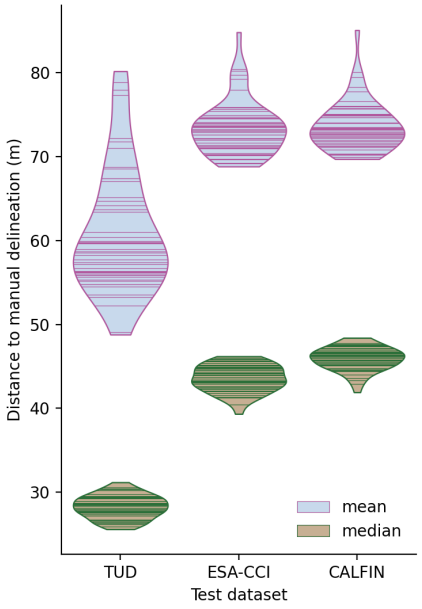

Figure 4. Accuracy assessment for the three independent test datasets. Every horizontal line inside the 'violin graphs' represents one of the 50 trained model applied to the test dataset. The vertical extent of each graph is defined by the corresponding minimum and maximum values.

Table 1. Results of the accuracy assessment. Given are the average minimal distance and the Hausdorff distance for the TUD, ESA-CCI and CALFIN test set. For both estimates we provide mean and median values. The standard deviations result from the 50 different models.

Test datast	Average minimal distance		Hausdorff distance	
	Mean (m)	Median (m)	Mean (m)	Median (m)
TUD	61.2 ± 7.5	28.3 ± 1.4	283.9 ± 28.1	156.4 ± 7.2
ESA-CCI	73.7 ± 2.9	45.9 ± 1.4	352.4 ± 14.1	205.4 ± 10.3
CALFIN	73.5 ± 3.3	43.6 ± 1.6	233.9 ± 5.7	162.9 ± 4.8

~~error is below the accuracy level of manual digitization which was estimated by Goliber et al. (2022) to be using~~ Overall, the mean average minimal distance errors are comparable to the results from Cheng et al. (2021) and (Zhang et al., 2023) who estimated who estimated 86.7 ± 1.4 m and 79 m, respectively. Table 1 gives the corresponding statistics.

In addition to the average minimal distance estimate we also calculate the Hausdorff distance (Huttenlocher et al., 1993). The Hausdorff distance only considers the greatest distance of all minimum distances along the two trajectories. As longer fronts are more likely to include misclassified parts, this measure tends to be larger for longer fronts. Goliber et al. (2022) applied the median Hausdorff distance to duplicated delineation from different authors ~~.~~ in order to estimate the accuracy level of manual digitization. Depending on the paired authors this manual delineation error varies between 59 m and 7350 m, with an average of

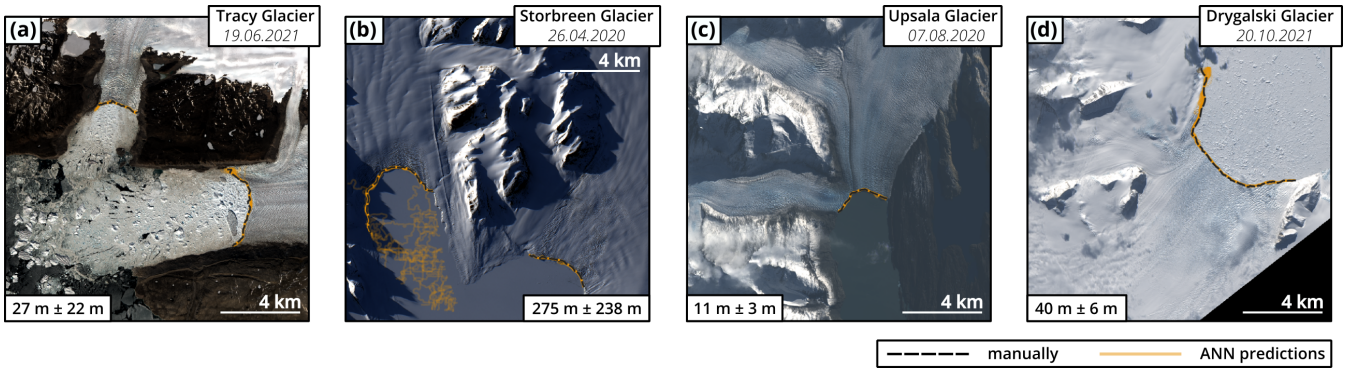

Figure 5. Test results for example glaciers which are outside the training dataset. Specifically of (a) Tracy Glacier in Greenland, (b) Storebreen in Svalbard, (c) Upsala Glacier in Paragonia and (d) Drygalski Glacier in Antarctica. Orange lines show the predictions from our 50 models. Overlap of lines is indicated by higher color intensity. The average minimal distance metric for each scene is given in meters. Landsat-8 imagery courtesy of the U.S. Geological Survey.

107 m. The median Hausdorff distances calculated for our test data is therefore within the range of manual delineation errors, but slightly larger than the overall author-to-author error of 107 m calculated by Goliber et al. (2022). Altogether, the quality of calving fronts delineated by our ANN model is comparable to that of manually delineated calving fronts.

3.2 Spatial transferability

In addition to the accuracy assessment over the entire test data set, we evaluate the degree of model generalisation and hence the spatial transferability of our method. Out of our 200 test scenes, 61 scenes are from glaciers that are not included in the training data. For these 61 test scenes over our 50 trained models, we calculate a mean (and median) average minimal distance error of 71.3 ± 19.4 m (median: 24.6 ± 2.1 m). This test error is larger than the error over the entire test set, at 61.2 ± 7.5 m. It is thus also larger than the error over the 139 test scenes of glaciers that are part of the training set, at 56.0 ± 5.3 m (median: 30.3 ± 1.7 m). Notably, we see not only a larger test error, but also a higher standard deviation between the models. This is due to a lower success rate and the resulting high error for individual predictions in cases where the ANN failed to locate the calving front.

Figure 5 gives the test results for four example scenes. Depicted glaciers are outside the training dataset. The calving fronts of Tracy Glacier (Fig. 5a), Upsala Glacier (Fig. 5c) and Drygalski Glacier (Fig. 5d) are reliably extracted with low distances to the manually delineated reference, and low deviation among all trained models. The accuracy is comparable to that of glaciers within the training data set. In contrast, the extractions for Storbreen Glacier (Fig. 5b, left) have a large error and high deviation among the trained models. The calving front is not delineated reliably. This could be due to a combination of the difficult lighting and the snow covered sea ice, which is a condition that might not be adequately represented in the training data. Interestingly, the calving front of the neighboring Hornbreen Glacier (Fig. 5b, bottom right) is extracted accurately over all models.

Among the 61 test images outside the glaciers of the training dataset 57 have an average minimal distance error below 100m (93 %), compared to 178 out of 200 over the whole test dataset (89 %) and 121 out of 139 of test images of glaciers that are included in the training set (87 %). Overall, this assessment confirms the spatial transferability of our processing system. However, the accuracy is lower compared to the extraction from glaciers that were included in the training data. Similar findings have been reported by previous studies (Baumhoer et al., 2019; Cheng et al., 2021; Zhang et al., 2023).

4 Results

4.1 Data product for Greenland from 2013 to 2021

Having trained and ~~validated~~ tested the ANN model, we apply our processing to Landsat-8 imagery in order to generate temporally dense calving front time series for 23 Greenland outlet glaciers. In doing so, we ~~process all but completely clouded Landsat scenes~~ download Landsat-8 imagery acquired between March 2013 and December 2021. ~~Failed~~ Images with cloud cover larger than 20 % and all Systematic Terrain Correction (L1GT) scenes are manually checked before downloading. Depending of the glacier 51 % (for Ingia Isbræ) to 63 % (for Helheim Glacier) of the available satellite scenes are discarded before download. After ANN processing, failed calving front extractions ~~,~~ are discarded. Calving front extraction fails when the predicted coastline trajectory does not intersect the static mask. Finally, calving fronts are filtered using the time series. For this we separate all entries with an area difference of larger than $1\,\mathrm{km}^2$ to both the previous and the ~~percentage of which varies between 5~~next entry. Separated entries are checked manually. Out of the 10587 satellite scenes processed by our ANN, 1344 calving front predictions (13 ~~% and 10 % depending on the glacier, are then manually~~%) were discarded. Figure ~~5~~ 6 gives a tabular overview of the final data product (for locations see Figure ~~2~~1). In total, we provide 9243 calving front lines, mostly achieving sub-weekly sampling outside polar night. Due to overlapping satellite orbits, glaciers in north, northeast and northwest Greenland undergo up to six image acquisitions per week depending on weather and season. Since we use optical data in this study our time series has observation gaps during polar nights. Depending on latitude, this gap lasts about one month for glaciers in south Greenland and up to three months for glaciers in north Greenland.

4.2 Long term, seasonal and subseasonal calving front changes

Marine terminating glaciers experience calving front variations at different time scales. While long-term changes are easy to resolve using already available data products, our time series offers unique opportunities to analyze seasonal and sub-seasonal terminus changes. To quantify these calving front changes we apply the well-established rectilinear box method (Moon and Joughin, 2008). Rather than using a single profile to measure advance or retreat this method adopts a rectilinear box, thus accounting for uneven changes along the calving front. Figure ~~6~~ 7 shows the method applied to our calving front time series for Jakobshavn Isbræ which is separated ~~here~~ into a northern and a southern branch. The inferred calving front variation exhibits a pronounced annual pattern combined with smaller sub-seasonal fluctuations. For comparison, the derived time series of the manually delineated ~~ESA-CCI~~ ESA-CCI product is shown. Although both datasets agree very well when it comes to comparing

	Kangiata Nunaata Sermia	Helheim Glacier	Kangerdlussuaq Glacier	Jakobshavn Isbræ	Sermeq Avangnardleq	Store Glacier	Rink Isbræ	Daugaard Jensen Glacier	Ingia Isbræ	Upernavik Isstrøm	Waltershausen Glacier	Hayes Glacier	Sverdrup Glacier	Kong Oscar Glacier	Dæcker Smith Glacier	Harald Molke Bræ	Tracy Glacier	Humboldt Glacier	Zachariae Isstrøm	Nioghalvfjerdsbræ	Hagen Bræ	Academy Glacier	Ryder Glacier	
2013	5	13	19	15	13	18	20	13	18	6	13	13	14	9	4	16	19	7	15	20	51	54	43	4
2014	23	33	42	29	33	40	43	30	30	19	18	33	38	26	25	41	46	32	46	38	66	60	53	Entries
2015	19	24	29	29	32	39	45	26	33	40	25	42	53	44	42	51	58	36	42	40	118	128	100	
2016	17	29	38	26	29	37	44	38	44	33	28	46	48	38	42	51	54	45	60	62	127	127	105	
2017	13	27	39	25	32	36	40	30	41	36	29	40	46	44	38	50	47	38	68	56	126	112	88	
2018	17	17	40	25	35	40	37	29	38	33	39	46	45	34	37	52	54	40	60	50	135	89	114	
2019	15	35	47	34	37	43	46	42	49	46	46	64	60	48	57	54	51	48	73	62	103	99	98	
2020	13	29	40	25	31	35	37	28	47	43	30	40	56	44	53	52	58	47	52	48	93	82	107	135
2021	23	31	43	30	29	33	52	56	44	37	41	46	59	48	44	50	49	33	42	64	116	108	86	
Total	145	238	337	238	271	321	364	292	344	293	269	370	419	335	342	417	436	326	458	440	935	859	794	9243

Figure 6. Temporal coverage of our ANN generated time series. The numbers and the color intensity indicate the amount of processed calving front positions in the respective year. Glaciers are sorted by latitude from south (left) to north (right).

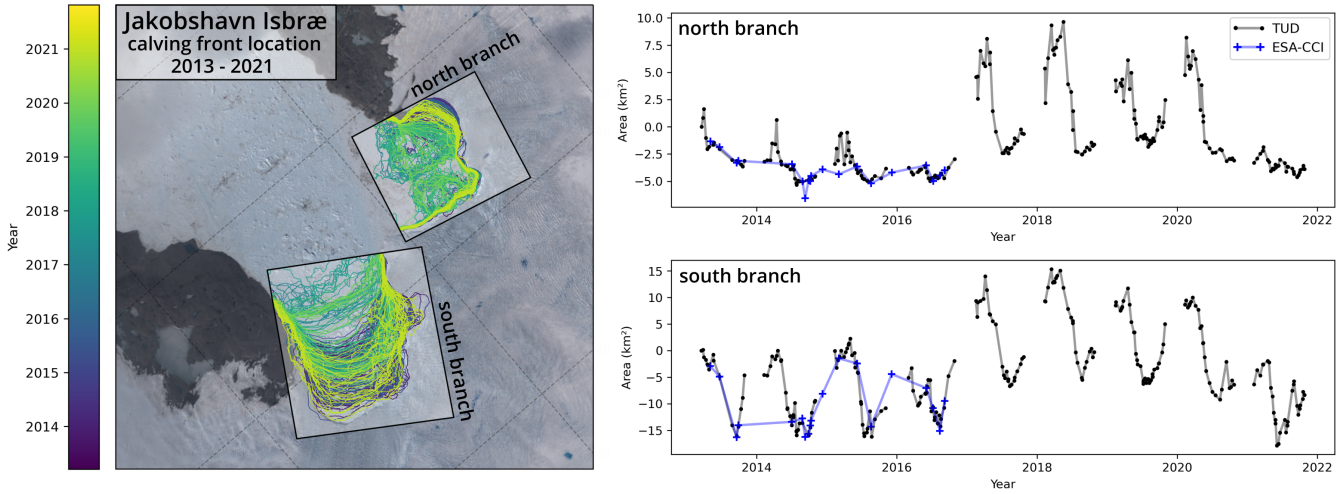

Figure 7. Rectilinear box method applied to the ANN generated calving front time series for Jakobshavn Isbræ (west Greenland). The glacier, which is separated into a northern and a southern branch, and the calving fronts are shown on the left. The corresponding time series are depicted on the right. Here, calving front positions, expressed as a surface area, are marked by a dot. For the TUD product (black) solid lines connect frontal positions of each year. Time series from the ESA-CCI product (blue) are shown for comparison. Landsat-8 image courtesy of the U.S. Geological Survey.

singular epochs, the ESA-CCI time series does not reliably capture the temporal ~~variation~~variations. This is particularly evident for the year 2014 when a whole annual cycle is missed by the manually delineated product.

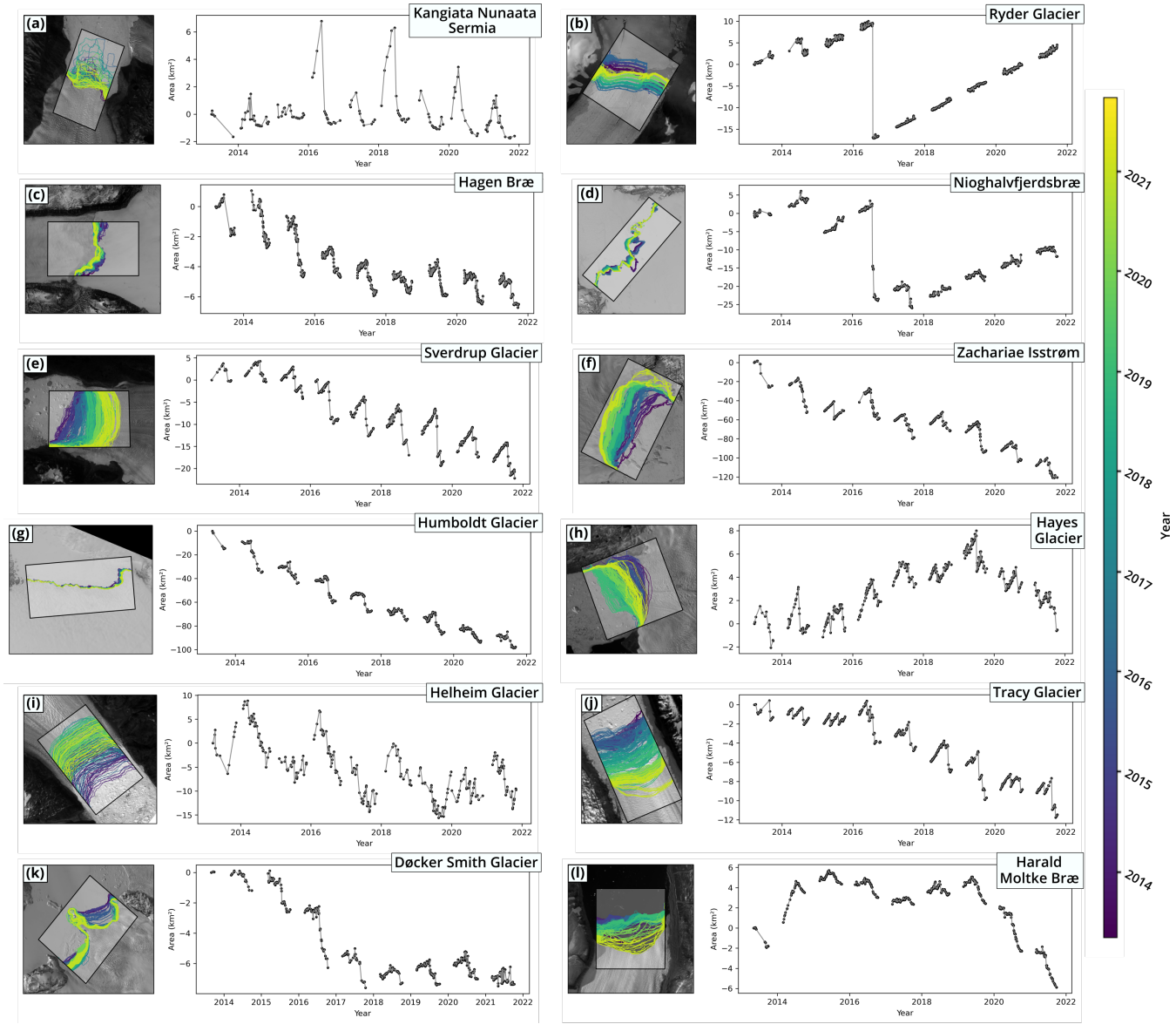

Figure 8. Example time series generated by our ANN algorithm for twelve Greenland glaciers. For each glacier a satellite image (left), containing the color-coded calving front trajectories, and the corresponding time series (right) are shown. Here, calving front positions are marked by black dots and solid lines connecting entries each year. Note that the ordinate axis is scaled differently for each glacier. Landsat-8 imagery courtesy of the U.S. Geological Survey.

Figure ~~7~~ 8 presents twelve more examples of our ANN generated time series. Most of these glaciers exhibit pronounced seasonal and sub-seasonal variations overlaid by a long-term signal. Except for Kangiata Nunaata Sermia (Fig. ~~7~~8a), Ryder Glacier (Fig. ~~7~~8b) and Hayes Glacier (Fig. ~~7~~8h), all example glaciers are retreating during the analysed time period. Notably, Zachariae

Isstrøm and Humboldt Glacier show an area loss of about $120\,\mathrm{km}^2$ and $100\,\mathrm{km}^2$ respectively. Ryder Glacier (Fig. ~~7~~8b) and Nioghalvfjerdsbræ (Fig. ~~7~~8d) are the only among the 23 glaciers in our study that do not undergo a pronounced seasonality. In those cases, the calving front variation is characterized by a steady advance and the sporadic detachment of large kilometer-sized icebergs. The date of detachment is precisely pinpointed by the time series. In the case of Nioghalvfjerdsbræ (Fig. ~~7~~8d), the time series also ~~separates two~~ resolves two separate break-offs that occurred in close succession. Other glacier time series, like Hayes Glacier (Fig. ~~7~~8h), Tracy Glacier (Fig. ~~7~~8j), Docker Smith Glacier (Fig. ~~7~~8k) and Harald Moltke Bræ (Fig. ~~7~~8l), reflect a change in calving rate during our observation period. For Harald Moltke Bræ (Fig. ~~7~~8l) the onset of this calving front retreat, starting 2019, coincides with the end of its six year-long surging phase and has already been anticipated by Müller et al. (2021).

4.3 Comparison to the CALFIN, AutoTerm and TermPicks data product

In addition to the data set produced in this study, there are two other automatic delineation products with a circum-Greenland coverage: the CALFIN data set by Cheng et al. (2021) and the AutoTerm repository by Zhang et al. (2023). Additionally, there is the TermPicks database (Goliber et al., 2022), which comprises manually delineated calving front data from 19 different authors. In this section, we will compare these three "big data" Greenland calving front datasets with the results of this study. The comparison takes place on three levels. Firstly, we compare the general statistics and scope. Secondly, we compare results over a reference period and reference glaciers defined according to their temporal and spatial overlap. Thirdly, we examine individual examples.

Table 2 (columns 2 to 4) presents the general statistics for the four datasets. Our data set covers a relatively short time span since we process imagery from the OLI and TIRS Landsat sensors, which have only been available since 2013. With 9243 mapped calving fronts over 23 glaciers our data product is smaller in both scope and size than the CALFIN, AutoTerm and TermPicks products. When examining the number of calving front traces, it is important to understand that the definition of what a single calving front contains varies from study to study. For instance, a single data entry in our dataset for the Upernavik Isstrøm includes four calving front features. CALFIN lists three separate calving fronts for the same glacier, and AutoTerm and Termpicks list two. For Jakobshavn Isbræ, CALFIN considers the north and south branch separately, while in our data set they are counted as one calving front. In addition, some of our predictions also include smaller neighboring glaciers that are located on the same image tile (e. g. Farquhar Glacier which is included together with Tracy Glacier or Akullersuup Sermia which is included together with Kangiata Nunaata Sermia). Usually, this applies to glaciers of a single glacier system that were previously connected. When counting shape file features, the number of entries in our data product contains 15150 entries.

To better compare differences in processing strategy, we define a reference period and reference glaciers by considering the temporal (2013 to 2019) and spatial overlap (13 glaciers) of the four data sets. These glaciers are: Kangiata Nunaata Sermia, Helheim Glacier, Kangerdlugssuaq Glacier, Jakobshavn Isbræ, Sermeq Avangnardleq, Store Glacier, Rink Isbrae, Ingia Isbræ, Upernavik Isstrøm, Hayes Glacier, Sverdrup Glacier, Kong Oscar Glacier and Døcker Smith Glacier. Within this reference we looked at mapped fronts, sampling rate and unique entries. Results are given in Table 2 (columns 5 to 7). We consider only one calving front entry per day and per glacier. Effectively, this removes (1) duplicate delineations of the same scene

Table 2. Comparison of the CALFIN, AutoTerm, TermPicks product as well as the data product presented in this study. The reference period (2013 to 2019) and the reference glaciers (13 glaciers) are defined by the temporal and spatial overlap of the four data products.

Dataset	Glaciers	Mapped fronts	Time span	Reference period and glaciers		
				Mapped fronts	Sampling rate (yr^{-1})	Unique entries
This study (Loebel et al., 2023)	23	9243	2013-2021	3005	33.02	372
CALFIN (Cheng et al., 2021)	66	22678	1972-2019	1322	14.53	15
AutoTerm (Zhang et al., 2023)	295	278239	1984-2021	7220	79.34	3724
TermPicks (Goliber et al., 2022)	278	39060	1948-2021	2287	25.13	505

(e. g. from multiple authors in the TermPicks data base or from the reference data which is included in CALFIN data set) and (2) inconsistencies in what constitutes a single calving front entry. Although having the same Landsat data basis our data product achieves a higher sampling rate and more unique front extractions than CALFIN. This is likely due to differences in input feature selection and processing. AutoTerm has the most mapped and unique fronts as well as the highest sampling rate. This is mainly due to its data basis which included Landsat, Sentinel-2 and Sentinel-1. Overall, 372 out of the 3005 calving fronts extracted by our method within the reference were not extracted by CALFIN, AutoTerm or TermPicks although all use Landsat-8 imagery.

Figure 9 shows the time series of CALFIN, AutoTerm and TermPicks compared to our study for four individual glaciers. To maximise the sampling of the different data sets, we analyse a centre line profile instead of using the box method. The mean distance for same-day calving front acquisitions d is indicated for each pair of time series. When examining these four examples, we observe a generally good agreement between the time series. Significant differences exist only for Humboldt Glacier (Fig. 9d). Here, the data quality of the AutoTerm product seems to be notably worse than for the other glaciers, with large fluctuations up to 5 km in distance. This may be attributed to the glacier front's large size, which, at least in our method, required additional processing steps. For Kangiata Nunaata Sermia (Fig. 9b) our data product is the only one which captures the signal from the seasonal ice tongue (Motyka et al., 2017; Moyer et al., 2017). This is reflected on the one hand in gaps in the other data sets and on the other hand in a higher distance for some same-day acquisitions. Although Landsat imagery is available, both CALFIN and AutoTerm have almost no calving front traces during the emergence, presence and disintegration of this seasonal ice tongue. We suspect, that the multi-spectral input information of our processing leads to a better extraction rate for scenes under these challenging conditions. All four examples highlight the varying sampling rates of the data products. In particular, the AutoTerm dataset has not only the highest sampling rate but also coverage during polar night (see late 2017 in Fig. 9a and late 2017 in Fig. 9c). The sampling rate of the TermPicks repository is lower than that of the automated processing systems in these four examples.

Compared to CALFIN, AutoTerm and TermPicks, our data product has the shortest time frame, lowest coverage and smallest amount of overall mapped calving front traces. However, due to different processing and the addition of multi-spectral input information our method is able to extract a significant amount of calving fronts, 13 % within the reference, that could not

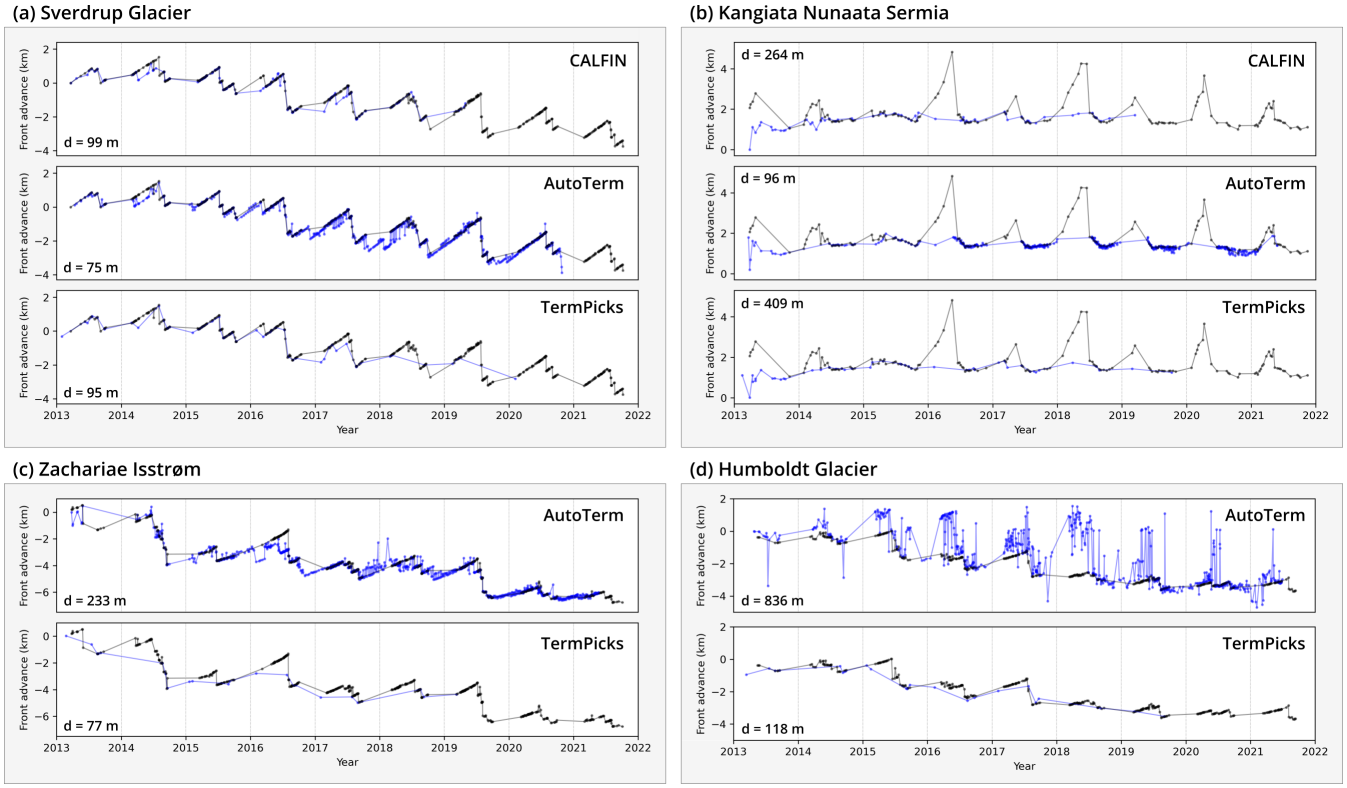

Figure 9. Comparison of the CALFIN, AutoTerm, TermPicks product (blue) to the data product presented in this study (black) for four example glaciers. Time series are derived along the central flow line of the glacier. Every comparison specifies the mean distance d between calving front delineations at identical days.

be extracted by the other methods. Importantly, these 13 % include extractions under challenging image conditions. For the analyzed reference, our method has a temporal resolution second only to that of the AutoTerm product, which benefits from multi-sensor input imagery. Overall, this comparison also presents a clear argument for the benefits of having multiple data products on glacier calving fronts. Current data products differ in scope but also differ for duplicate extractions for identical glacier front traces, often exceeding estimated delineation uncertainties. A better understanding of these differences is crucial and requires further investigation. As a final point, we want to emphasise the potential of combining different glacier front products. Greene et al. (2024) have demonstrated the advantages of such a combination for large-scale glaciological analyses.

5 Discussion

Changes in calving front position are, along with other observables like ice velocity and elevation change, part of a complex feedback cycle between a glacier and its environment. ~~In discussing our results, we present a first application of our temporally high-resolution calving front information. In particular, we infer valuable insights into glacier dynamics by linking changes~~

~~in calving front position to bedrock topography.~~ Long-term calving front trends of Greenland glaciers are well characterised (Howat and Eddy, 2011; King et al., 2020; Fahrner et al., 2021; Black and Joughin, 2022; Greene et al., 2024). However, about 80 % of Greenland glaciers also experience terminus changes on a seasonal and subseasonal basis (Black and Joughin, 2023) . Of the 23 glaciers analysed in this study, 19 glaciers show a clear seasonality between 2013 and 2021. As observed by other studies (Joughin et al., 2008b; Seale et al., 2011; Carr et al., 2013; Schild and Hamilton, 2013; Murray et al., 2015; Moon et al., 2015; Cas , glacier retreat typically starts in late spring with retreat rates peaking in late summer. A number of mechanisms have been identified as controls for these seasonal terminus changes. These include the duration and timing of meltwater runoff (Sohn et al., 1998; Nick et al., 2010; Chauche et al., 2014; Carroll et al., 2016; Fried et al., 2018; Wood et al., 2021), changes in buttressing force by sea ice and ice melange (Howat et al., 2010; Carr et al., 2013; Todd and Christoffersen, 2014; Cassotto et al., 2015; Mo , basal sliding (De Juan et al., 2010; Moon et al., 2015) and ocean driven melt (Motyka et al., 2003; Bevan et al., 2012a; Chauche et al., 20 . When a glacier is forced into a state of retreat, both the rate and pattern of retreat are modulated by the subglacial topography. For marine terminating glaciers in Greenland, this effect has been studied (Warren, 1991; Warren and Glasser, 1992; Joughin et al., 2008b; and modelled (Enderlin et al., 2013; Morlighem et al., 2016; Choi et al., 2017) intensively. In particular, faster retreat rates were found to be associated with overdeepening and retrograde topography.

The new generation of automatically delineated calving front data products not only facilitates glaciological analysis in terms of significant time savings, but may also provide new insights due to the high temporal resolution and spatial coverage. Figure ~~8~~ 10 shows our calving front time series for three example glaciers in relation to bedrock elevation, taken from the BedMachine Greenland ~~model (Morlighem, 2022), for four example glaciers. Interaction between calving front variation and bedrock topography for (a) Ingia Isbræ, (b) Upernavik Isstrøm C, (c) Daugaard Jensen Glacier and (d) Kangerdlugssuaq Glacier. Shown are (from left to right) a satellite image with calving front trajectories as well as a marked profile, bedrock topography and color-coded calving front positions along this profile and the corresponding time series of calving front variation. Note that the axis are scaled differently for each glacier. Landsat-8 imagery courtesy of the U.S. Geological Survey.~~ Version 5 model (Morlighem, 2022). Profiles extend from point A to point B along a central flowline. The calving front of Ingia Isbræ (Fig. ~~8~~10a) retreated from 2013 to the end of 2017 by 3.2 km (8.6 km^2 in area) with a pronounced seasonal pattern. ~~This~~ Due to retrograde topography (at ~4 km in Fig. 10a), this retreat is particularly rapid in ~~2017 and 2018. We suspect this is due to retrograde topography.~~ 2016 and 2017. Since 2018, the calving front ~~is located~~ has been in a topographic minimum. ~~This seems to prevent a fast retreat and significantly reduces the~~ , preventing further retreat and reducing seasonal amplitude. ~~In the case of Upernavik Isstrøm C~~ These observations confirm the analysis of Catania et al. (2018), which described the continuous retreat of Ingia Isbræ from 2002 to 2016 and suggested further retreat by more than 1 km until the calving front stabilises on the prograde bed topography. The calving front change of Kangerdlugssuaq Glacier (Fig. ~~8b) , there was a rapid decline in 2014 and 2015, which has slowed considerably since the end of 2015. This is probably a result of the prograde topography of the bedrock . In addition, the seasonal amplitude of the calving front change varies considerably, from a minimum of~~ 10b) shows high seasonal amplitudes as well as a significant retreat from 2016 to early 2018. With the exception of 2017 and 2018, where we observe a sustained retreat, the seasonal amplitude remains almost constant at around 4 km (~~in area) in 2020 to a maximum of (in area)in 2019. This could be related to the prograde bedrock slope, which leads to a floating and less stable glacier tongue~~

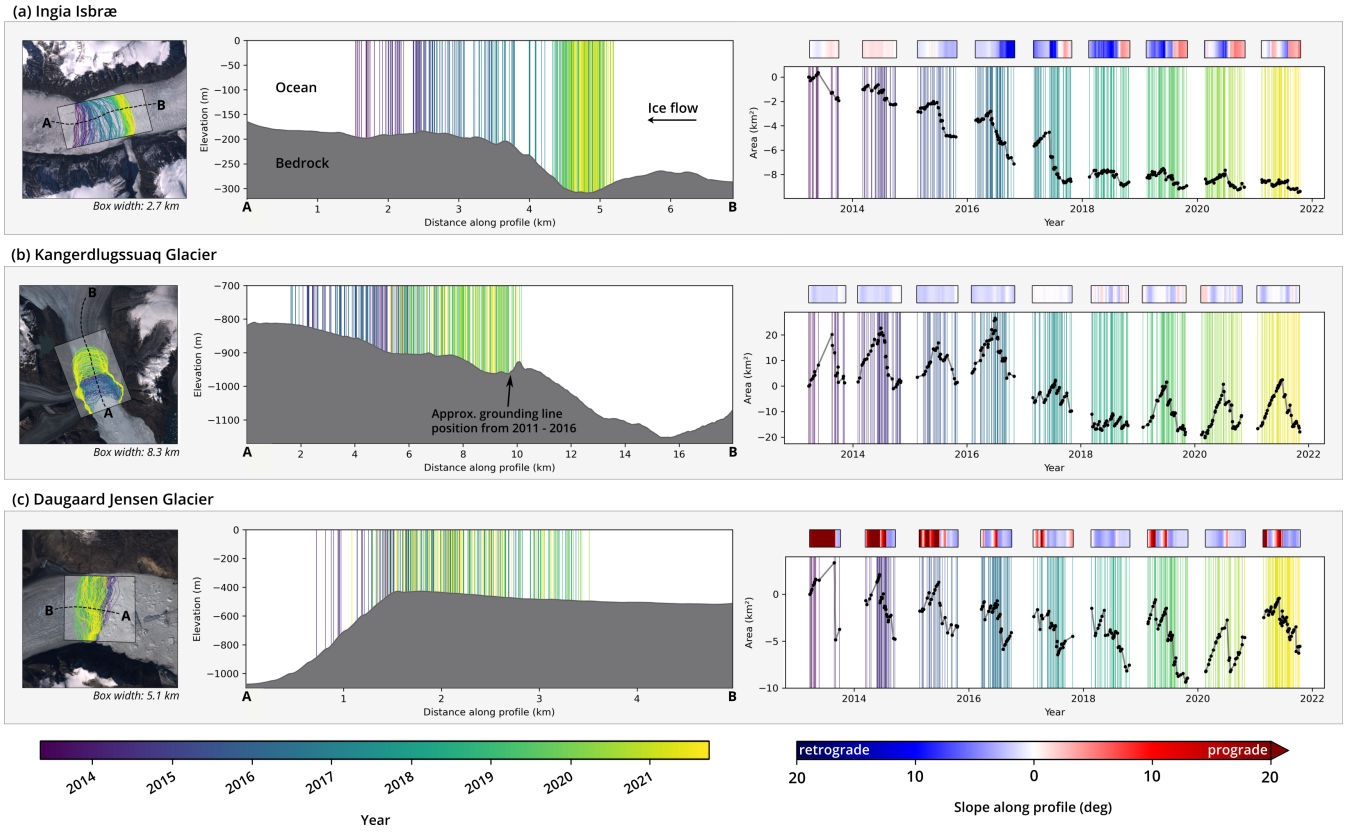

Figure 10. Effect of bedrock topography of calving front variation for (a) Ingia Isbræ, (b) Kangerdlugssuaq Glacier and (c) Daugaard Jensen Glacier. Shown are (from left to right) a satellite image with calving front trajectories as well as a marked profile, bedrock topography and color-coded calving front positions along this profile and the corresponding time series of calving front variation. Note that the axes are scaled differently for each glacier. Landsat-8 imagery courtesy of the U.S. Geological Survey.

~~during rapid glacier advance~~21 km^2 in area). This calving front pattern is also described by Kehrl et al. (2017). Furthermore, the authors show that Kangerdlugssuaq's grounding line has retreated in 2010 and 2011 to a stable bedrock position (bedrock bump at ~10 km in Fig. 10b), resulting in a floating ice tongue of ~5 km in length. Due to the retrograde bedrock topography after the bedrock bump (from 10 km to 15 km in Fig. 10b) and the reinitialization of the seasonal terminus pattern from 2019 to 2021, we suspect that the calving front retreat from 2016 to 2018 is coupled with a grounding line retreat on retrograde bed topography followed by a restabilisation further inland (likely at 15.5 km in Fig. 10b). This would confirm the second scenario suggested by Brough et al. (2019). The calving behavior of Daugaard Jensen Glacier (Fig. ~~8~~10c) is influenced by the abrupt change of bedrock slope ~~near~~ close to the frontal position. An advance beyond this point, from a slightly retrograde into a steeply prograde topography, ~~results in a floating ice tongue~~leads to a loss of basal drag and longitudinal stresses. This influences calving behaviour, and in particular ~~results in the calving of large tabular icebergs up to~~ favors calving of tabular icebergs like in 2013 (8.2 km^2 in size~~. The calving front change of Kangerdlugssuaq Glacier (Fig. 8d) shows high seasonal~~

amplitudes as well as a significant retreat from late 2016 to early 2018. With the exception of 2017 and 2018, where we observe a sustained retreat, the seasonal amplitude remains almost constant at around (in area). Our time series does not show long-term calving front changes since 2018. Considering the bed topography, it is apparent that the glacier front , which was at a stable position until late 2021, has the potential to retreat into a steeply retrograde topography. This retrograde topography continues for about upstream. If this tipping point is reached, an accelerated retreat of the glaciers' calving front location might be expected. These examples further highlight the benefits of the temporally high-resolution) and 2020 ($4.2\,\mathrm{km}^2$ in size). Although Daugaard Jensen's glacier front has remained roughly at this location for over 70 years (Stearns et al., 2005) and is considered to be stable (Bevan et al., 2012b), temporally high resolution calving front information is still necessary to resolve and understand these stable glacier dynamics. More generally, high temporal resolution calving front information not only allow to analyze glacier retreat and advance, but also to better differentiate between different calving styles and patterns. Long-term calving front trends are often superimposed by seasonal variability and sub-seasonal fluctuations. A separation of these signals is crucial for studying dynamic glacier changes and fully understand underlying processes.

6 Conclusions

This study presents a deep learning based processing system for automatic delineation of calving front locations from multi-spectral Landsat-8 imagery. Using three independent test datasets we validate the performance and spatial transferability of our processing system. The quality of the automatically extracted calving fronts is comparable to that of manually delineated calving fronts. By overcoming Our method enables a considerably higher extraction rate compared to other automation methods that use the same data basis. Importantly, this higher extraction rate is partly due to the ability to perform extractions under challenging cloud, illumination and ice mélange conditionswe make an important step forward to considerably enhancing both the temporal resolution as well as the coverage of our resulting time series. The time series derived by this processing system resolve long-term, seasonal and sub-seasonal calving front variations. This clearly surpasses the potential of manually delineated data products. Our resulting data product, which includes 9242 calving fronts over 23 Greenland glaciers, is therefore a valuable contribution to the existing data repositories.

The presented method and the resulting data product addresses address the needs of the glaciology community for a comprehensive parameterization of glacier calving in Greenland. The presented example time series highlight the high temporal resolution achieved by our deep learning method. Especially for longer calving fronts, dense sampling is not attainable using manual delineation. Thus, our time series provided for Humboldt time series derived by this processing system resolve long-term, seasonal and sub-seasonal calving front variations. The benefit is particularly significant for large glaciers where there is a lack of manual delineated data, such as Humbold Glacier, Zachariae Isstrøm and Nioghalvfjerdsbræ are, among many others, are of unprecedented temporal resolution, resolving their sub-seasonal calving front variability for the first timeNioghalvfjerdsbrae. Due to the spatial transferability of this method, our processing system has the potential to be applied to other marine-terminating glaciers around the world.

~~Although~~ By the time series presented in this paper, we give only a selected ~~and a rather narrow~~ glimpse into the dynamics of these glaciers~~, it is highly important to note that~~ . However, the demonstrated capability of automatically resolving the sub-seasonal calving front variations is an important step forward towards a spatially comprehensive ~~Greenland wide~~ Greenland-wide monitoring system. In conjunction with other components concerning ice flow, elevation change, solid earth response and hydrological processes, this will open up new opportunities to integratively assess, model and simulate dynamic ice sheet changes. Advancing towards this digital twin of the Greenland Ice Sheet will improve our understanding of its evolution and its role within the broader Earth climate system.

Intelligent processing strategies, like deep ANN, will play a major role in shaping the future of glacier monitoring and associated modelling tasks. This is especially true for analyzing the increasing amount of remote sensing imagery. Well-trained and thoroughly validated ANN will be state-of-the-art for automated calving front delineation. The results presented in this paper ~~do not only reinforce existing efforts of deep learning based calving front detection but also lay the foundation for future developments~~ will contribute to future advancements in this field.

7 ~~Data~~

6.1 ~~Data source~~

~~The presented processing system is based on optical Landsat-8 imagery. We use the orthorectified and radiometrically calibrated level 1 data products as provided by the United States Geological Survey (U.S. Geological Survey, 2023). Carrying two scientific instruments, the Operational Land Imager (OLI) and the Thermal Infrared Sensor (TIRS), Landsat-8 provides a particularly wide multispectral coverage. The eleven spectral bands comprise data from visible, near-infrared, short-wave infrared and thermal infrared wavelengths, from to . With exception to the panchromatic band and the two thermal bands, which have a spatial resolution of and respectively, all other bands have a resolution of . Apart from band 9, which is outside an atmospheric window and, therefore, intended for atmospheric observations, all available bands are used as input for our ANN. The integration of these multispectral bands leads to generally more accurate predictions than using conventional single-band inputs only, which has already been shown by Loebel et al. (2022). This is especially true for difficult illumination and ice-melange conditions.~~

6.1 ~~Reference dataset~~

~~We use manually delineated calving front locations as reference data. For model training, we use 698 calving front positions across 19 Greenland glaciers between 2013 and 2019. Glaciers are selected for their broad spatial distribution and diverse morphology as well as for different calving and ocean conditions. A spatial overview of all Greenland glaciers applied in this study is given in Figure 2. To test the model we apply three different testing sets. The TUD testing dataset includes four additional Greenland glaciers, Boydell and Drygalski Glacier at the Antarctic Peninsula, Storbreen Glacier in Svalbard as well as Upsala Glacier in Patagonia. In total, the TUD testing set contains 200 calving front positions across 27 glaciers from 2020~~

and 2021. In addition to our own testing data set we use manually delineated calving fronts from the ESA-CCI (ENVEO, 2017) and the CALFIN (Cheng et al., 2021) product. Here, we use all available calving front positions for our selected Greenland glaciers for which we find a corresponding Landsat-8 scene with less than 24 hours time difference. This results in additional 100 manually delineated calving front positions for the ESA-CCI and 110 for the CALFIN testing datasets.

7 Methods

6.1 Pre-Processing

To use the satellite data as input for the ANN requires pre-processing. In particular, we create stacked raster subsets from the multispectral satellite bands and the manually delineated calving front locations. These subsets have dimensions of px × 512 px with a unified ground sampling distance and are centered on the calving front of the respective glacier. For each multispectral band we apply an image enhancement in form of a cumulative count cut, clipping the data between the 0.1 and 98 percentile, counteracting overexposure in our satellite imagery. Additionally, all satellite bands are then normalized to the range between 0 and 1 using an 8-bit quantization. Corresponding manually delineated calving front positions, given either as a line string or polygon shape-file, are processed into binary raster masks segmenting land and glacier from ocean. Altogether, one stacked raster subset includes nine satellite bands and a matching ground truth mask.

6.1 Semantic image segmentation

To extract the calving front location from the input images we apply a convolutional neural network that performs a pixel-wise semantic image segmentation, separating a glacier-land class from a water class. In particular, we use a U-Net type architecture introduced by Ronneberger et al. (2015). This architecture consists of a contracting path, resembling a typical convolutional network where spatial resolution is reduced while feature information is increased, followed by an expanding path where feature and spatial information are combined. The receptive field of a U-Net is defined by the number of contracting and expanding blocks. As calving front extraction needs adequate spatial context (Heidler et al., 2021) in this study we enhance the U-Net by two additional resolution levels, i.e. from four to six. The applied processing architecture and the relevant dimensions are shown in Figure 9. **U-Net based model architecture used this study. Contracting sequences are composed of convolutions followed by batch normalization (BatchNorm), a rectified linear unit (ReLU) and a max pooling operation. An expanding sequence is built from a concatenation from the contracting path, convolutions followed by BatchNorm, a ReLU and an up-convolution. The specific dimensions are designated at the top of the blocks.** Our model is fitted using the pre-processed training data. Before initializing the model training we select every fifth image of the training dataset for internal validation. The remaining training data is augmented eightfold by rotating and flipping. Finally, the resulting 6208 raster subsets are used for fitting the model. For this, we use randomized batches of size eight and apply the Adam optimization algorithm (Kingma and Ba, 2014) on a binary cross-entropy loss function for a total of 200 epochs. Final model weights are selected based on the classification accuracy of the internal validation dataset. The ANN processing is implemented using the

TensorFlow 2.4 library (Abadi et al., 2015). Model training is carried out on an IBM Power 9 node and an NVIDIA V100 GPU with 32 GB high bandwidth memory. The training of one model requires about twelve hours with a main memory utilization of 80 GB and an average GPU power consumption of 265 W.

6.1 Post-Processing

As output of the ANN output we derive a floating point number probability mask where each image pixel is assigned a probability between 0 (water) and 1 (glacier and land). During post-processing we vectorize this probability mask using the Geospatial Data Abstraction Library (GDAL) contour algorithm (GDAL/OGR contributors, 2020) with a threshold of 0.5. Eventually, we extract the glacier's calving front by intersecting the vectorized coastline trajectory with a static mask. This mask is created manually for each glacier and specifies a corridor of possible calving front locations. Calving fronts exceeding the 512 px × 512 px window are split into multiple independent predictions which are then averaged in the overlapping area before vectorization. Applying this strategy, which is motivated by Baumhoer et al. (2019), Zachariae Isstrøm, Nioghalvfjerdsbræ and Humboldt Glacier are split into two, three and seven separate overlapping predictions, respectively.

7 Binary classification metrics

Although our model is fitted using pixel-wise binary cross-entropy the mean and median distances to manual delineation form the main error metric to validate our model. The reason for this is that a high binary classification performance does not necessarily lead to an accurate prediction of the calving front trajectory. The binary classification performance is most important for pixels at the glacier front but less relevant for the rest of the image. Nevertheless, in Table 1 we specify, along with the mean and median distance errors, the confusion matrix of our model accuracy assessment using the TUD test dataset. This confusion matrix enables to derive commonly used binary classification metrics like accuracy, precision, recall or F1-Score making our results more comparable with those of already existing studies. Results of the accuracy assessment. The mean and median distance to manual delineation and the confusion matrix for the glacier/land class are given. In addition, the standard deviation of the respective parameters is indicated. Example: Mean TP are all glacier/land image pixels of the test dataset that are correctly classified on average across all 50 models. (lr)2-3(lr)4-7Mean (m)Median (m)Mean TP Mean TN Mean FP Mean FN (lr)1-7TUD ESA-CCI CALFIN

Code and data availability. The following assets are published along with this article:

- The data product of automatically delineated calving front positions (format: ESRI shapefile), containing 9243 calving front positions across 23 Greenland outlet glaciers, is available at http://dx.doi.org/10.25532/OPARA-208 (Loebel et al., 2023).
- All reference data applied in this study is available at http://dx.doi.org/10.25532/OPARA-282 (Loebel et al., 2024). In particular, this includes 898 manually delineated calving front positions provided in a georeferenced shapefile format, as well as 1220 machine learning ready raster subsets (pre-processed, 9 channels) with their corresponding manual delineated segmentation mask.

- We provide a containerized implementation (platform: Docker) of the presented processing system. The software automatically extracts calving front positions from Landsat-8 or Landsat-9 Level-1 data archives for glaciers used within this study or at user-defined coordinates. This enables the analysis of glaciers that are outside our reference dataset or beyond the temporal frame of our study. The software is available at https://github.com/eloebel/glacier-front-extraction (last access 24 March 2023) and https://doi.org/10.5281/zenodo.7755774 (Loebel, 2023a).
- Our implementation (software: Python 3) of the rectilinear box method is available at https://github.com/eloebel/rectilinear-box-method (last access 24 March 2023) and https://doi.org/10.5281/zenodo.7738605 (Loebel, 2023b).

Author contributions. EL designed the study, developed the methodology, carried out the data processing and time series generation. MS and MH supervised the work and provided direction for the overall study. AH and JS provided key input for the discussion. KH and XXZ contributed to the neural network processing and accuracy assessment. CL assisted in creating the reference dataset. All authors discussed the results and contributed to writing the manuscript.

Competing interests. The author declares that there are no competing interests.

Acknowledgements. We would like to thank the USGS for providing Landsat imagery. Also, we are grateful to the TU Dresden computing centre (ZIH) for providing their high-performance computing and storage infrastructure. We acknowledge the National Snow and Ice Data Center QGreenland package. This work was supported by the Helmholtz Association of German Research Centers as part of the Helmholtz Information and Data Science Incubator, project ”Artificial Intelligence for Cold Regions” (AI-CORE, grant no. ZT-I-0016), ~~and~~ by the German Federal Ministry of Education and Research (BMBF), project "Greenland Ice Sheet/Ocean Interaction" (GROCE2, grant no. 03F0778G) and by the German Federal Ministry for Economic Affairs and Climate Action in the framework of the "national center of excellence ML4Earth" (grant no. 50EE2201C) .

References

Abadi, M., Agarwal, A., Barham, P., Brevdo, E., Chen, Z., Citro, C., Corrado, G. S., Davis, A., Dean, J., Devin, M., Ghemawat, S., Goodfellow, I., Harp, A., Irving, G., Isard, M., Jia, Y., Jozefowicz, R., Kaiser, L., Kudlur, M., Levenberg, J., Mané, D., Monga, R., Moore, S., Murray, D., Olah, C., Schuster, M., Shlens, J., Steiner, B., Sutskever, I., Talwar, K., Tucker, P., Vanhoucke, V., Vasudevan, V., Viégas, F., Vinyals, O., Warden, P., Wattenberg, M., Wicke, M., Yu, Y., and Zheng, X.: TensorFlow: Large-Scale Machine Learning on Heterogeneous Systems, https://www.tensorflow.org/, software available from tensorflow.org, 2015.

Andersen, J. A., Fausto, R. S., Hansen, K., Box, J. E., Andersen, S. B., Ahlstrøm, A. P., van As, D., Citterio, M., Colgan, W., Karlsson, N. B., Kjeldsen, K. K., Korsgaard, N. J., Larsen, S. H., Mankoff, K. D., Pedersen, A. Ø., Shields, C. L., Solgaard, A., and Vandecrux, B.: Update of annual calving front lines for 47 marine terminating outlet glaciers in Greenland (1999–2018), GEUS Bulletin, 43, https://doi.org/10.34194/GEUSB-201943-02-02, (last access: 11.November 2021), 2019.

Baumhoer, C. A., Dietz, A. J., Kneisel, C., and Kuenzer, C.: Automated Extraction of Antarctic Glacier and Ice Shelf Fronts from Sentinel-1 Imagery Using Deep Learning, Remote Sensing, 11, 2529, https://doi.org/10.3390/rs11212529, 2019.

Benn, D. I., Cowton, T., Todd, J., and Luckman, A.: Glacier Calving in Greenland, Current Climate Change Reports, 3, 282 – 290, https://doi.org/10.1007/s40641-017-0070-1, 2017.

Bevan, S. L., Luckman, A. J., and Murray, T.: Glacier dynamics over the last quarter of a century at Helheim, Kangerdlugssuaq and 14 other major Greenland outlet glaciers, The Cryosphere, 6, 923–937, 2012a.

Bevan, S. L., Murray, T., Luckman, A. J., Hanna, E., and Huybrechts, P.: Stable dynamics in a Greenland tidewater glacier over 26 years despite reported thinning, Annals of Glaciology, 53, 241–248, 2012b.

Black, T. E. and Joughin, I.: Multi-decadal retreat of marine-terminating outlet glaciers in northwest and central-west Greenland, The Cryosphere, 16, 807–824, https://doi.org/10.5194/tc-16-807-2022, https://tc.copernicus.org/articles/16/807/2022/, 2022.

Black, T. E. and Joughin, I.: Weekly to monthly terminus variability of Greenland's marine-terminating outlet glaciers, The Cryosphere, 17, 1–13, https://doi.org/10.5194/tc-17-1-2023, https://tc.copernicus.org/articles/17/1/2023/, 2023.

Bondizo, J. H., Morlighem, M., Seroussi, H., Kleiner, T., Rückamp, M., Mouginot, J., Moon, T., Larour, E. Y., and Humbert, A.: The mechanisms behind Jakobshavn Isbræ's acceleration and mass loss: A 3-D thermomechanical model study, Geophysical Research Letters, 44, 6252–6260, https://doi.org/10.1002/2017GL073309, 2017.

Brough, S., Carr, J. R., Ross, N., and Lea, J. M.: Exceptional retreat of Kangerlussuaq Glacier, east Greenland, between 2016 and 2018, Frontiers in Earth Science, 7, 123, 2019.

Bunce, C., Carr, J. R., Nieoew, P. W., Ross, N., and Killick, R.: Ice front change of marine-terminating outlet glaciers in northwest and southeast Greenland during the 21st century, Journal of Glaciology, 64, 523–535, https://doi.org/10.1017/jog.2018.44, 2018.

Carr, J. R., Vieli, A., and Stokes, C.: Influence of sea ice decline, atmospheric warming, and glacier width on marine-terminating outlet glacier behavior in northwest Greenland at seasonal to interannual timescales, Journal of Geophysical Research: Earth Surface, 118, 1210–1226, 2013.

Carr, J. R., Vieli, A., Stokes, C., Jamieson, S., Palmer, S., Christoffersen, P., Dowdeswell, J., Nick, F., Blankenship, D., and Young, D.: Basal topographic controls on rapid retreat of Humboldt Glacier, northern Greenland, Journal of Glaciology, 61, 137–150, 2015.

Carroll, D., Sutherland, D. A., Hudson, B., Moon, T., Catania, G. A., Shroyer, E. L., Nash, J. D., Bartholomaus, T. C., Felikson, D., Stearns, L. A., et al.: The impact of glacier geometry on meltwater plume structure and submarine melt in Greenland fjords, Geophysical Research Letters, 43, 9739–9748, 2016.

Cassotto, R., Fahnestock, M., Amundson, J. M., Truffer, M., and Joughin, I.: Seasonal and interannual variations in ice melange and its impact on terminus stability, Jakobshavn Isbræ, Greenland, Journal of Glaciology, 61, 76–88, 2015.

Catania, G., Stearns, L., Sutherland, D., Fried, M., Bartholomaus, T., Morlighem, M., Shroyer, E., and Nash, J.: Geometric controls on tidewater glacier retreat in central western Greenland, Journal of Geophysical Research: Earth Surface, 123, 2024–2038, 2018.

Chauche, N., Hubbard, A., Gascard, J.-C., Box, J. E., Bates, R., Koppes, M., Sole, A., Christoffersen, P., and Patton, H.: Ice–ocean interaction and calving front morphology at two west Greenland tidewater outlet glaciers, The Cryosphere, 8, 1457–1468, 2014.

Cheng, D., Hayes, W., Larour, E., Mohajerani, Y., Wood, M., Velicogna, I., and Rignot, E.: Calving Front Machine (CALFIN): Glacial Termini Dataset and Automated Deep Learning Extraction Method for Greenland, 1972–2019 , The Cryosphere, 15, https://doi.org/10.5194/tc-15-1663-2021, 2021.

Choi, Y., Morlighem, M., Rignot, E., Mouginot, J., and Wood, M.: Modeling the response of Nioghalvfjerdsfjorden and Zachariae Isstrøm glaciers, Greenland, to ocean forcing over the next century, Geophysical Research Letters, 44, 11–071, 2017.

Cook, S. J., Christoffersen, P., Truffer, M., Chudley, T. R., and Abellán, A.: Calving of a Large Greenlandic Tidewater Glacier has Complex Links to Meltwater Plumes and Mélange, Journal of Geophysical Research: Earth Surface, 126, e2020JF006 051, https://doi.org/https://doi.org/10.1029/2020JF006051, 2021.

Davari, A., Baller, C., Seehaus, T., Braun, M., Maier, A., and Christlein, V.: Pixelwise Distance Regression for Glacier Calving Front Detection and Segmentation, IEEE Transactions on Geoscience and Remote Sensing, 60, 1–10, https://doi.org/10.1109/TGRS.2022.3158591, 2022a.

Davari, A., Islam, S., Seehaus, T., Hartmann, A., Braun, M., Maier, A., and Christlein, V.: On Mathews Correlation Coefficient and Improved Distance Map Loss for Automatic Glacier Calving Front Segmentation in SAR Imagery, IEEE Transactions on Geoscience and Remote Sensing, 60, 1–12, https://doi.org/10.1109/TGRS.2021.3115883, 2022b.

De Juan, J., Elósegui, P., Nettles, M., Larsen, T. B., Davis, J. L., Hamilton, G. S., Stearns, L. A., Andersen, M. L., Ekström, G., Ahlstrøm, A. P., et al.: Sudden increase in tidal response linked to calving and acceleration at a large Greenland outlet glacier, Geophysical Research Letters, 37, 2010.

Edwards, T. L., Nowicki, S., Marzeion, B., Hock, R., Goelzer, H., Seroussi, H., Jourdain, N. C., Slater, D. A., Turner, F. E., Smith, C. J., McKenna, C. M., Simon, E., Abe-Ouchi, A., Gregory, J. M., Larour, E., Lipscomb, W. H., Payne, A. J., Shepherd, A., Agosta, C., Alexander, P., Albrecht, T., Anderson, B., Asay-Davis, X., Aschwanden, A., Barthel, A., Bliss, A., Calov, R., Chambers, C., Champollion, N., Choi, Y., Cullather, R., Cuzzone, J., Dumas, C., Felikson, D., Fettweis, X., Fujita, K., Galton-Fenzi, B. K., Gladstone, R., Golledge, N. R., Greve, R., Hattermann, T., Hoffman, M. J., Humbert, A., Huss, M., Huybrechts, P., Immerzeel, W., Kleiner, T., Kraaijenbrink, P., Le clec'h, S., Lee, V., Leguy, G. R., Little, C. M., Lowry, D. P., Malles, J.-H., Martin, D. F., Maussion, F., Morlighem, M., O'Neill, J. F., Nias, I., Pattyn, F., Pelle, T., Price, S. F., Quiquet, A., Radić, V., Reese, R., Rounce, D. R., Rückamp, M., Sakai, A., Shafer, C., Schlegel, N.-J., Shannon, S., Smith, R. S., Straneo, F., Sun, S., Tarasov, L., Trusel, L. D., Van Breedam, J., van de Wal, R., van den Broeke, M., Winkelmann, R., Zekollari, H., Zhao, C., Zhang, T., and Zwinger, T.: Projected land ice contributions to twenty-first-century sea level rise, Nature, 593, 74–82, https://doi.org/10.1038/s41586-021-03302-y, 2021.

Enderlin, E. M., Howat, I. M., and Vieli, A.: High sensitivity of tidewater outlet glacier dynamics to shape, The Cryosphere, 7, 1007–1015, 2013.

ENVEO: Greenland Calving Front Dataset, 1990–2016, v3.0, http://products.esa-icesheets-cci.org/products/downloadlist/CFL, (last access: 11.November 2021), 2017.

Fahrner, D., Lea, J. M., Brough, S., Mair, D. W. F., and Abermann, J.: Linear response of the Greenland ice sheet's tidewater glacier terminus positions to climate, Journal of Glaciology, 67, 193–203, https://doi.org/10.1017/jog.2021.13, 2021.

Felikson, D., A Catania, G., Bartholomaus, T. C., Morlighem, M., and Noël, B. P.: Steep glacier bed knickpoints mitigate inland thinning in Greenland, Geophysical Research Letters, 48, e2020GL090 112, 2021.

Fried, M., Catania, G., Stearns, L., Sutherland, D., Bartholomaus, T., Shroyer, E., and Nash, J.: Reconciling drivers of seasonal terminus advance and retreat at 13 Central West Greenland tidewater glaciers, Journal of Geophysical Research: Earth Surface, 123, 1590–1607, 2018.

GDAL/OGR contributors: GDAL/OGR Geospatial Data Abstraction software Library, Open Source Geospatial Foundation, https://gdal.org, 2020.

Goelzer, H., Nowicki, S., Payne, A., Larour, E., Seroussi, H., Lipscomb, W. H., Gregory, J., Abe-Ouchi, A., Shepherd, A., Simon, E., Agosta, C., Alexander, P., Aschwanden, A., Barthel, A., Calov, R., Chambers, C., Choi, Y., Cuzzone, J., Dumas, C., Edwards, T., Felikson, D., Fettweis, X., Golledge, N. R., Greve, R., Humbert, A., Huybrechts, P., Le clec'h, S., Lee, V., Leguy, G., Little, C., Lowry, D. P., Morlighem, M., Nias, I., Quiquet, A., Rückamp, M., Schlegel, N.-J., Slater, D. A., Smith, R. S., Straneo, F., Tarasov, L., van de Wal, R., and van den Broeke, M.: The future sea-level contribution of the Greenland ice sheet: a multi-model ensemble study of ISMIP6, The Cryosphere, 14, 3071–3096, https://doi.org/10.5194/tc-14-3071-2020, https://tc.copernicus.org/articles/14/3071/2020/, 2020.

Goliber, S., Black, T., Catania, G., Lea, J. M., Olsen, H., Cheng, D., Bevan, S., Bjørk, A., Bunce, C., Brough, S., Carr, J. R., Cowton, T., Gardner, A., Fahrner, D., Hill, E., Joughin, I., Korsgaard, N. J., Luckman, A., Moon, T., Murray, T., Sole, A., Wood, M., and Zhang, E.: TermPicks: a century of Greenland glacier terminus data for use in scientific and machine learning applications, The Cryosphere, 16, 3215–3233, https://doi.org/10.5194/tc-16-3215-2022, https://tc.copernicus.org/articles/16/3215/2022/, 2022.

Gourmelon, N., Seehaus, T., Braun, M., Maier, A., and Christlein, V.: Calving fronts and where to find them: a benchmark dataset and methodology for automatic glacier calving front extraction from synthetic aperture radar imagery, Earth System Science Data, 14, 4287–4313, https://doi.org/10.5194/essd-14-4287-2022, https://essd.copernicus.org/articles/14/4287/2022/, 2022.

Greene, C. A., Gardner, A. S., Wood, M., and Cuzzone, J. K.: Ubiquitous acceleration in Greenland Ice Sheet calving from 1985 to 2022, Nature, 625, 523–528, 2024.

Heidler, K., Mou, L., Baumhoer, C., Dietz, A., and Zhu, X. X.: HED-UNet: Combined Segmentation and Edge Detection for Monitoring the Antarctic Coastline, IEEE Transactions on Geoscience and Remote Sensing, 2021.

Heidler, K., Mou, L., Loebel, E., Scheinert, M., Lefèvre, S., and Zhu, X. X.: Deep Active Contour Models for Delineating Glacier Calving Fronts, in: IGARSS 2022 - 2022 IEEE International Geoscience and Remote Sensing Symposium, pp. 4490–4493, https://doi.org/10.1109/IGARSS46834.2022.9884819, 2022.

Heidler, K., Mou, L., Loebel, E., Scheinert, M., Lefèvre, S., and Zhu, X. X.: A Deep Active Contour Model for Delineating Glacier Calving Fronts, IEEE Transactions on Geoscience and Remote Sensing, 2023.

Herrmann, O., Gourmelon, N., Seehaus, T., Maier, A., Fürst, J. J., Braun, M. H., and Christlein, V.: Out-of-the-box calving-front detection method using deep learning, The Cryosphere, 17, 4957–4977, https://doi.org/10.5194/tc-17-4957-2023, https://tc.copernicus.org/articles/17/4957/2023/, 2023.

Horwath, M., Gutknecht, B. D., Cazenave, A., Palanisamy, H. K., Marti, F., Marzeion, B., Paul, F., Le Bris, R., Hogg, A. E., Otosaka, I., Shepherd, A., Döll, P., Cáceres, D., Müller Schmied, H., Johannessen, J. A., Nilsen, J. E. Ø., Raj, R. P., Forsberg, R., Sandberg Sørensen, L., Barletta, V. R., Simonsen, S. B., Knudsen, P., Andersen, O. B., Ranndal, H., Rose, S. K., Merchant, C. J., Macintosh, C. R., von Schuckmann, K., Novotny, K., Groh, A., Restano, M., and Benveniste, J.: Global sea-level budget and ocean-mass budget, with a focus on

advanced data products and uncertainty characterisation, Earth System Science Data, 14, 411–447, https://doi.org/10.5194/essd-14-411-2022, https://essd.copernicus.org/articles/14/411/2022/, 2022.

Howat, I. M. and Eddy, A.: Multi-decadal retreat of Greenland's marine-terminating glaciers, Journal of Glaciology, 57, 389–396, https://doi.org/10.3189/002214311796905631, 2011.

Howat, I. M., Box, J. E., Ahn, Y., Herrington, A., and McFADDEN, E. M.: Seasonal variability in the dynamics of marine-terminating outlet glaciers in Greenland, Journal of Glaciology, 56, 601–613, 2010.

Huttenlocher, D., Klanderman, G., and Rucklidge, W.: Comparing images using the Hausdorff distance, IEEE Transactions on Pattern Analysis and Machine Intelligence, 15, 850–863, https://doi.org/10.1109/34.232073, 1993.

Joughin, I., Howat, I., Alley, R. B., Ekstrom, G., Fahnestock, M., Moon, T., Nettles, M., Truffer, M., and Tsai, V. C.: Ice-front variation and tidewater behavior on Helheim and Kangerdlugssuaq Glaciers, Greenland, Journal of Geophysical Research: Earth Surface, 113, https://doi.org/10.1029/2007JF000837, 2008a.

Joughin, I., Howat, I. M., Fahnestock, M., Smith, B., Krabill, W., Alley, R. B., Stern, H., and Truffer, M.: Continued evolution of Jakobshavn Isbrae following its rapid speedup, Journal of Geophysical Research: Earth Surface, 113, 2008b.

Joughin, I., Moon, T., and Black, T.: MEaSUREs Annual Greenland Outlet Glacier Terminus Positions from SAR Mosaics, Version 1, Boulder, Colorado USA. NASA National Snow and Ice Data Center Distributed Active Archive Center, https://doi.org/10.5067/DC0MLBOCL3EL, (last access: 11.November 2021), 2015.

Kehrl, L. M., Joughin, I., Shean, D. E., Floricioiu, D., and Krieger, L.: Seasonal and interannual variabilities in terminus position, glacier velocity, and surface elevation at Helheim and Kangerlussuaq Glaciers from 2008 to 2016, Journal of Geophysical Research: Earth Surface, 122, 1635–1652, 2017.

King, M. D., Howat, I. M., Jeong, S., Noh, M. J., Wouters, B., Noël, B., and van den Broeke, M. R.: Seasonal to decadal variability in ice discharge from the Greenland Ice Sheet, The Cryosphere, 12, 3813–3825, https://doi.org/10.5194/tc-12-3813-2018, https://tc.copernicus.org/articles/12/3813/2018/, 2018.

King, M. D., Howat, I. M., Candela, S. G., Noh, M. J., Jeong, S., Noël, B. P., van den Broeke, M. R., Wouters, B., and Negrete, A.: Dynamic ice loss from the Greenland Ice Sheet driven by sustained glacier retreat, Communications Earth & Environment, 1, 1–7, https://doi.org/10.1038/s43247-020-0001-2, 2020.

Kingma, D. P. and Ba, J.: Adam: A Method for Stochastic Optimization, arXiv preprint arXiv:1412.6980, 2014.

Kneib-Walter, A., Lüthi, M. P., Moreau, L., and Vieli, A.: Drivers of recurring seasonal cycle of glacier calving styles and patterns, Frontiers in Earth Science, 9, 667 717, 2021.

Krieger, L. and Floricioiu, D.: Automatic calving front delienation on TerraSAR-X and Sentinel-1 SAR imagery, International Geoscience and Remote Sensing Symposium (IGARSS), https://doi.org/10.1109/IGARSS.2017.8127584, 2017.

Liu, H. and Jezek, K. C.: A Complete High-Resolution Coastline of Antarctica Extracted from Orthorectified Radarsat SAR Imagery, Photogrammetric Engineering and Remote Sensing, 5, 605 – 616, https://doi.org/10.14358/PERS.70.5.605, 2004.

Liu, J., Enderlin, E. M., Marschall, H.-P., and Khalil, A.: Automated Detection of Marine Glacier Calving Fronts Using the 2-D Wavelet Transform Modulus Maxima Segmentation Method, IEEE Transactions on Geoscience and Remote Sensing, 59, 9047 – 9056, https://doi.org/10.1109/TGRS.2021.3053235, 2021.

Loebel, E.: eloebel/glacier-front-extraction: Initial release v1.0.0 [code], Zenodo, https://doi.org/10.5281/zenodo.7755774, 2023a.

Loebel, E.: eloebel/rectilinear-box-method: Initial release v1.0.0 [code], Zenodo, https://doi.org/10.5281/zenodo.7738605, 2023b.

Loebel, E., Scheinert, M., Horwath, M., Heidler, K., Christmann, J., Phan, L. D., Humbert, A., and Zhu, X. X.: Extracting Glacier Calving Fronts by Deep Learning: The Benefit of Multispectral, Topographic, and Textural Input Features, IEEE Transactions on Geoscience and Remote Sensing, 60, 1–12, https://doi.org/10.1109/TGRS.2022.3208454, 2022.

Loebel, E., Scheinert, M., Horwath, M., Humbert, A., Sohn, J., Heidler, K., Liebezeit, C., and Zhu, X. X.: Data product of Greenland glacier calving front locations delineated by deep learning, 2013 to 2021 [data set], TU Dresden OpARA, https://doi.org/http://dx.doi.org/10.25532/OPARA-208, 2023.

Loebel, E., Scheinert, M., Horwath, M., Humbert, A., Sohn, J., Heidler, K., Liebezeit, C., and Zhu, X. X.: Manually delineated glacier calving front locations of 27 marine-terminating glaciers from 2013 to 2021 [data set], TU Dresden OpARA, https://doi.org/http://dx.doi.org/10.25532/OPARA-282, 2024.

Lüthi, M. P., Vieli, A., Moreau, L., Joughin, I., Reisser, M., Small, D., and Stober, M.: A century of geometry and velocity evolution at Eqip Sermia, West Greenland, Journal of Glaciology, 62, 640–654, 2016.

Marochov, M., Stokes, C. R., and Carbonneau, P. E.: Image classification of marine-terminating outlet glaciers in Greenland using deep learning methods, The Cryosphere, 15, 5041–5059, https://doi.org/10.5194/tc-15-5041-2021, https://tc.copernicus.org/articles/15/5041/2021/, 2021.

Melton, S. M., Alley, R. B., Anandakrishnan, S., Parizek, B. R., Shahin, M. G., Stearns, L. A., LeWinter, A. L., and Finnegan, D. C.: Meltwater drainage and iceberg calving observed in high-spatiotemporal resolution at Helheim Glacier, Greenland, Journal of Glaciology, p. 1–17, https://doi.org/10.1017/jog.2021.141, 2022.

Mohajerani, Y., Wood, M., Velicogna, I., and Rignot, E.: Detection of Glacier Calving Margins with Convolutional Neural Networks: A Case Study , Remote Sensing, 11, 74, https://doi.org/10.3390/rs11010074, 2019.

Moon, T. and Joughin, I.: Changes in ice front position on Greenland's outlet glaciers from 1992 to 2007, Journal of Geophysical Research: Earth Surface, 113, https://doi.org/10.1029/2007JF000927, 2008.

Moon, T., Joughin, I., and Smith, B.: Seasonal to multiyear variability of glacier surface velocity, terminus position, and sea ice/ice mélange in northwest Greenland, Journal of Geophysical Research: Earth Surface, 120, 818–833, 2015.

Moon, T., Fisher, M., Simonoko, H., and Stafford, T.: QGreenland (v2.0.0) [software], https://doi.org/10.5281/zenodo.6369184, https://qgreenland.org, 2022.

Morlighem, M., Bondzio, J., Seroussi, H., Rignot, E., Larour, E., Humbert, A., and Rebuffi, S.: Modeling of Store Gletscher's calving dynamics, West Greenland, in response to ocean thermal forcing, Geophysical Research Letters, 43, 2659–2666, 2016.

Morlighem, M., Williams, C. N., Rignot, E., An, L., Arndt, J. E., Bamber, J. L., Catania, G., Chauché, N., Dowdeswell, J. A., Dorschel, B., Fenty, I., Hogan, K., Howat, I., Hubbard, A., Jakobsson, M., Jordan, T. M., Kjeldsen, K. K., Millan, R., Mayer, L., Mouginot, J., Noël, B. P. Y., O'Cofaigh, C., Palmer, S., Rysgaard, S., Seroussi, H., Siegert, M. J., Slabon, P., Straneo, F., van den Broeke, M. R., Weinrebe, W., Wood, M., and Zinglersen, K. B.: BedMachine v3: Complete Bed Topography and Ocean Bathymetry Mapping of Greenland From Multibeam Echo Sounding Combined With Mass Conservation, Geophysical Research Letters, 44, 11 051 – 11 061, https://doi.org/10.1002/2017GL074954, 2017.

Morlighem, M., Wood, M., Seroussi, H., Choi, Y., and Rignot, E.: Modeling the response of northwest Greenland to enhanced ocean thermal forcing and subglacial discharge, The Cryosphere, 13, 723–734, https://doi.org/10.5194/tc-13-723-2019, https://tc.copernicus.org/articles/13/723/2019/, 2019.

Morlighem, M. e. a.: IceBridge BedMachine Greenland, Version 5, https://doi.org/10.5067/GMEVBWFLWA7X, https://nsidc.org/data/IDBMG4/versions/5, 2022.

Motyka, R. J., Hunter, L., Echelmeyer, K. A., and Connor, C.: Submarine melting at the terminus of a temperate tidewater glacier, LeConte Glacier, Alaska, USA, Annals of Glaciology, 36, 57–65, 2003.

Motyka, R. J., Cassotto, R., Truffer, M., Kjeldsen, K. K., Van As, D., Korsgaard, N. J., Fahnestock, M., Howat, I., Langen, P. L., Mortensen, J., and et al.: Asynchronous behavior of outlet glaciers feeding Godthåbsfjord (Nuup Kangerlua) and the triggering of Narsap Sermia's retreat in SW Greenland, Journal of Glaciology, 63, 288–308, https://doi.org/10.1017/jog.2016.138, 2017.

Mouginot, J., Rignot, E., Bjørk, A. A., Van den Broeke, M., Millan, R., Morlighem, M., Noël, B., Scheuchl, B., and Wood, M.: Forty-six years of Greenland Ice Sheet mass balance from 1972 to 2018, Proceedings of the national academy of sciences, 116, 9239–9244, 2019.

Moyer, A. N., Nienow, P. W., Gourmelen, N., Sole, A. J., and Slater, D. A.: Estimating Spring Terminus Submarine Melt Rates at a Greenlandic Tidewater Glacier Using Satellite Imagery, Frontiers in Earth Science, 5, https://doi.org/10.3389/feart.2017.00107, https://www.frontiersin.org/articles/10.3389/feart.2017.00107, 2017.

Murray, T., Scharrer, K., Selmes, N., Booth, A. D., James, T. D., Bevan, S. L., Bradley, J., Cook, S., Llana, L. C., Drocourt, Y., et al.: Extensive retreat of Greenland tidewater glaciers, 2000–2010, Arctic, antarctic, and alpine research, 47, 427–447, 2015.

Müller, L., Horwath, M., Scheinert, M., Mayer, C., Ebermann, B., Floricioiu, D., Krieger, L., Rosenau, R., and Vijay, S.: Surges of Harald Moltke Bræ, north-western Greenland: seasonal modulation and initiation at the terminus, The Cryosphere, 15, 3355 – 3375, https://doi.org/10.5194/tc-15-3355-2021, 2021.

Nick, F. M., Van der Veen, C. J., Vieli, A., and Benn, D. I.: A physically based calving model applied to marine outlet glaciers and implications for the glacier dynamics, Journal of Glaciology, 56, 781–794, 2010.

Otosaka, I. N., Shepherd, A., Ivins, E. R., Schlegel, N.-J., Amory, C., van den Broeke, M. R., Horwath, M., Joughin, I., King, M. D., Krinner, G., Nowicki, S., Payne, A. J., Rignot, E., Scambos, T., Simon, K. M., Smith, B. E., Sørensen, L. S., Velicogna, I., Whitehouse, P. L., A, G., Agosta, C., Ahlstrøm, A. P., Blazquez, A., Colgan, W., Engdahl, M. E., Fettweis, X., Forsberg, R., Gallée, H., Gardner, A., Gilbert, L., Gourmelen, N., Groh, A., Gunter, B. C., Harig, C., Helm, V., Khan, S. A., Kittel, C., Konrad, H., Langen, P. L., Lecavalier, B. S., Liang, C.-C., Loomis, B. D., McMillan, M., Melini, D., Mernild, S. H., Mottram, R., Mouginot, J., Nilsson, J., Noël, B., Pattle, M. E., Peltier, W. R., Pie, N., Roca, M., Sasgen, I., Save, H. V., Seo, K.-W., Scheuchl, B., Schrama, E. J. O., Schröder, L., Simonsen, S. B., Slater, T., Spada, G., Sutterley, T. C., Vishwakarma, B. D., van Wessem, J. M., Wiese, D., van der Wal, W., and Wouters, B.: Mass balance of the Greenland and Antarctic ice sheets from 1992 to 2020, Earth System Science Data, 15, 1597–1616, https://doi.org/10.5194/essd-15-1597-2023, https://essd.copernicus.org/articles/15/1597/2023/, 2023.

Periyasamy, M., Davari, A., Seehaus, T., Braun, M., Maier, A., and Christlein, V.: How to Get the Most Out of U-Net for Glacier Calving Front Segmentation, IEEE Journal of Selected Topics in Applied Earth Observations and Remote Sensing, 15, 1712–1723, https://doi.org/10.1109/JSTARS.2022.3148033, 2022.

Robel, A. A.: Thinning sea ice weakens buttressing force of iceberg mélange and promotes calving, Nature Communications, 8, 14 596, 2017.

Ronneberger, O., Fischer, P., and Brox, T.: U-Net: Convolutional Networks for Biomedical Image Segmentation, In: Navab N., Hornegger J., Wells W., Frangi A. (eds) Medical Image Computing and Computer-Assisted Intervention – MICCAI 2015., 9351, 234–241, https://doi.org/10.1007/978-3-319-24574-4_28, 2015.

Rosenau, R.: Untersuchung von Fließgeschwindigkeit und Frontlage der großen Ausflussgletscher Grönlands mittels multitemporaler Landsat-Aufnahmen, Ph.D. thesis, Technische Universität Dresden, Qucosa, urn:nbn:de:bsz:14-qucosa-138514, 2014.

Rückamp, M., Goelzer, H., and Humbert, A.: Sensitivity of Greenland ice sheet projections to spatial resolution in higher-order simulations: the Alfred Wegener Institute (AWI) contribution to ISMIP6 Greenland using the Ice-sheet and Sea-level System Model (ISSM), The Cryosphere, 14, 3309–3327, https://doi.org/10.5194/tc-14-3309-2020, https://tc.copernicus.org/articles/14/3309/2020/, 2020.

Sakakibara, D. and Sugiyama, S.: Seasonal ice-speed variations in 10 marine-terminating outlet glaciers along the coast of Prudhoe Land, northwestern Greenland, Journal of Glaciology, 66, 25–34, 2020.

Schild, K. M. and Hamilton, G. S.: Terminus position time series: Helheim and Kangerdlugssuaq glaciers, Greenland, Arctic Data Center, https://doi.org/10.18739/A2W93G, 2013.

Seale, A., Christoffersen, P., Mugford, R. I., and O'Leary, M.: Ocean forcing of the Greenland Ice Sheet: Calving fronts and patterns of retreat identified by automatic satellite monitoring of eastern outlet glaciers, Journal of Geophysical Research: Earth Surface, 116, https://doi.org/10.1029/2010JF001847, 2011.

Sohn, H. G. and Jezek, K. C.: Mapping ice sheet margins from ERS-1 SAR and SPOT imagery, International Journal of Remote Sensing, 20, 3201 – 3216, https://doi.org/10.1080/014311699211705, 1999.

Sohn, H.-G., Jezek, K. C., and van der Veen, C. J.: Jakobshavn Glacier, West Greenland: 30 years of spaceborne observations, Geophysical Research Letters, 25, 2699–2702, 1998.

Stearns, L. A., Hamilton, G. S., and Reeh, N.: Multi-decadal record of ice dynamics on Daugaard Jensen Gletscher, East Greenland, from satellite imagery and terrestrial measurements, Annals of Glaciology, 42, 53–58, https://doi.org/10.3189/172756405781812565, 2005.

The IMBIE Team: Mass balance of the Greenland Ice Sheet from 1992 to 2018, Nature, pp. 233 – 239, https://doi.org/10.1038/s41586-019-1855-2, 2020.

Todd, J. and Christoffersen, P.: Are seasonal calving dynamics forced by buttressing from ice mélange or undercutting by melting? Outcomes from full-Stokes simulations of Store Glacier, West Greenland, The Cryosphere, 8, 2353–2365, 2014.

Trevers, M., Payne, A. J., Cornford, S. L., and Moon, T.: Buoyant forces promote tidewater glacier iceberg calving through large basal stress concentrations, The Cryosphere, 13, 1877–1887, https://doi.org/10.5194/tc-13-1877-2019, https://tc.copernicus.org/articles/13/1877/2019/, 2019.

U.S. Geological Survey: USGS EarthExplorer, https://earthexplorer.usgs.gov/, (last access: 13.March 2023), 2023.

Vieli, A. and Nick, F. M.: Understanding and Modelling Rapid Dynamic Changes of Tidewater Outlet Glaciers: Issues and Implications, Surveys in Geophysics volume, 32, 437 – 458, https://doi.org/10.1007/s10712-011-9132-4, 2011.

Warren, C. R.: Terminal environment, topographic control and fluctuations of West Greenland glaciers, Boreas, 20, 1–15, 1991.

Warren, C. R. and Glasser, N. F.: Contrasting response of South Greenland glaciers to recent climatic change, Arctic and Alpine Research, pp. 124–132, 1992.

Wood, M., Rignot, E., Fenty, I., An, L., Bjørk, A., van den Broeke, M., Cai, C., Kane, E., Menemenlis, D., Millan, R., et al.: Ocean forcing drives glacier retreat in Greenland, Science Advances, 7, eaba7282, 2021.

Wu, F., Gourmelon, N., Seehaus, T., Zhang, J., Braun, M., Maier, A., and Christlein, V.: AMD-HookNet for Glacier Front Segmentation, IEEE Transactions on Geoscience and Remote Sensing, 61, 1–12, 2023.

Zhang, E., Liu, L., and Huang, L.: Automatically delineating the calving front of Jakobshavn Isbræ from multitemporal TerraSAR-X images: a deep learning approach, The Cryosphere, 13, 1729–1741, https://doi.org/10.5194/tc-13-1729-2019, 2019.

Zhang, E., Liu, L., Huang, L., and Ng, K. S.: An automated, generalized, deep-learning-based method for delineating the calving fronts of Greenland glaciers from multi-sensor remote sensing imagery, Remote Sensing of Environment, 254, 112 265, https://doi.org/10.1016/j.rse.2020.112265, 2021.

Zhang, E., Catania, G., and Trugman, D. T.: AutoTerm: an automated pipeline for glacier terminus extraction using machine learning and a “big data” repository of Greenland glacier termini, The Cryosphere, 17, 3485–3503, https://doi.org/10.5194/tc-17-3485-2023, https://tc.copernicus.org/articles/17/3485/2023/, 2023.

Zhu, X. X., Tuia, D., Mou, L., Xia, G.-S., Zhang, L., Xu, F., and Frauendorfer, F.: Deep Learning in Remote Sensing: A Comprehensive Review and List of Resources, IEEE Geoscience and Remote Sensing Magazine, 5, 8–36, https://doi.org/10.1109/MGRS.2017.2762307, 2017.